



**HAL**  
open science

## Harvesting of Prebiotic Fructooligosaccharides by Nonbeneficial Human Gut Bacteria

Zhi Wang, Alexandra S. Tauzin, Elisabeth Laville, Pietro Tedesco, Fabien Letisse, Nicolas Terrapon, Pascale Lepercq, Myriam Mercade, Gabrielle Potocki-Veronese

► **To cite this version:**

Zhi Wang, Alexandra S. Tauzin, Elisabeth Laville, Pietro Tedesco, Fabien Letisse, et al.. Harvesting of Prebiotic Fructooligosaccharides by Nonbeneficial Human Gut Bacteria. *mSphere*, 2020, 5 (1), 26 p. 10.1128/mSphere.00771-19 . hal-02478442

**HAL Id: hal-02478442**

**<https://hal.science/hal-02478442v1>**

Submitted on 13 Feb 2020


**HAL** is a multi-disciplinary open access archive for the deposit and dissemination of scientific research documents, whether they are published or not. The documents may come from teaching and research institutions in France or abroad, or from public or private research centers.

L'archive ouverte pluridisciplinaire **HAL**, est destinée au dépôt et à la diffusion de documents scientifiques de niveau recherche, publiés ou non, émanant des établissements d'enseignement et de recherche français ou étrangers, des laboratoires publics ou privés.



Distributed under a Creative Commons Attribution 4.0 International License

# Harvesting of Prebiotic Fructooligosaccharides by Nonbeneficial Human Gut Bacteria

Zhi Wang,<sup>a</sup> Alexandra S. Tauzin,<sup>a</sup> Elisabeth Laville,<sup>a</sup> Pietro Tedesco,<sup>a</sup> Fabien Létisse,<sup>a</sup>  Nicolas Terrapon,<sup>b,c</sup> Pascale Lepercq,<sup>a</sup> Myriam Mercade,<sup>a</sup>  Gabrielle Potocki-Veronese<sup>a</sup>

<sup>a</sup>TBI, CNRS, INRA, INSAT, Université de Toulouse, Toulouse, France

<sup>b</sup>AFMB, UMR 7257 CNRS, Aix-Marseille Université, Marseille, France

<sup>c</sup>INRA, USC 1408 AFMB, Marseille, France

**ABSTRACT** Prebiotic oligosaccharides, such as fructooligosaccharides, are increasingly being used to modulate the composition and activity of the gut microbiota. However, carbohydrate utilization analyses and metagenomic studies recently revealed the ability of deleterious and uncultured human gut bacterial species to metabolize these functional foods. Moreover, because of the difficulties of functionally profiling transmembrane proteins, only a few prebiotic transporters have been biochemically characterized to date, while carbohydrate binding and transport are the first and thus crucial steps in their metabolism. Here, we describe the molecular mechanism of a phosphotransferase system, highlighted as a dietary and pathology biomarker in the human gut microbiome. This transporter is encoded by a metagenomic locus that is highly conserved in several human gut *Firmicutes*, including *Dorea* species. We developed a generic strategy to deeply analyze, *in vitro* and *in cellulo*, the specificity and functionality of recombinant transporters in *Escherichia coli*, combining carbohydrate utilization locus and host genome engineering and quantification of the binding, transport, and growth rates with analysis of phosphorylated carbohydrates by mass spectrometry. We demonstrated that the *Dorea* fructooligosaccharide transporter is specific for kestose, whether for binding, transport, or phosphorylation. This constitutes the biochemical proof of effective phosphorylation of glycosides with a degree of polymerization of more than 2, extending the known functional diversity of phosphotransferase systems. Based on these new findings, we revisited the classification of these carbohydrate transporters.

**IMPORTANCE** Prebiotics are increasingly used as food supplements, especially in infant formulas, to modify the functioning and composition of the microbiota. However, little is currently known about the mechanisms of prebiotic recognition and transport by gut bacteria, while these steps are crucial in their metabolism. In this study, we established a new strategy to profile the specificity of oligosaccharide transporters, combining microbiomics, genetic locus and strain engineering, and state-of-the-art metabolomics. We revisited the transporter classification database and proposed a new way to classify these membrane proteins based on their structural and mechanistic similarities. Based on these developments, we identified and characterized, at the molecular level, a fructooligosaccharide transporting phosphotransferase system, which constitutes a biomarker of diet and gut pathology. The deciphering of this prebiotic metabolism mechanism by a nonbeneficial bacterium highlights the controversial use of prebiotics, especially in the context of chronic gut diseases.

**KEYWORDS** *Dorea*, chronic gut diseases, fructooligosaccharides, microbiome, phosphotransferase system

**Citation** Wang Z, Tauzin AS, Laville E, Tedesco P, Létisse F, Terrapon N, Lepercq P, Mercade M, Potocki-Veronese G. 2020. Harvesting of prebiotic fructooligosaccharides by nonbeneficial human gut bacteria. *mSphere* 5:e00771-19. <https://doi.org/10.1128/mSphere.00771-19>.

**Editor** Vincent B. Young, University of Michigan—Ann Arbor

**Copyright** © 2020 Wang et al. This is an open-access article distributed under the terms of the [Creative Commons Attribution 4.0 International license](https://creativecommons.org/licenses/by/4.0/).

Address correspondence to Gabrielle Potocki-Veronese, [veronese@insa-toulouse.fr](mailto:veronese@insa-toulouse.fr).

**Received** 24 October 2019

**Accepted** 9 December 2019

**Published** 8 January 2020

Prebiotics are functional foods, defined as “nondigestible compounds that, through their metabolization by microorganisms in the gut, modulate composition and/or activity of the gut microbiota, thus conferring a beneficial physiological effect on the host” (1–3). Inulin and fructooligosaccharides (FOS), comprising  $\beta(2\rightarrow1)$  fructosyl units linked to sucrose, are universally agreed to be prebiotic fibers. They are naturally present in a variety of plants such as Jerusalem artichoke, wheat, barley, rye, onions, garlic, asparagus, and banana (4, 5). They are increasingly used as food supplements, especially in infant formulas (5, 6), with the global inulin and FOS markets estimated to exceed \$5.8 billion by 2024 (7, 8). Numerous studies indicate that inulin and FOS are selectively fermented by human gut bifidobacteria and lactobacilli, inducing beneficial effects for the host, such as facilitating defecation and reducing endotoxemia, insulin resistance, and colon cancer risks (9–12). Notwithstanding this evidence and the commercial interest, some nonbeneficial gut bacterial species (13, 14), such as *Dorea longicatena*, a species associated with several pathologies such as irritable bowel syndrome (IBS) (15, 16), have been shown to feed on these compounds. Moreover, abdominal pain in IBS is alleviated by limiting the consumption of fermentable oligo-, di-, and monosaccharides and polyols (FODMAPs) such as FOS, resulting in a decrease in *Bacteroides*, *Ruminococcaceae*, *Faecalibacterium*, and *Dorea* species in the gut microbiota composition (17). In addition, the abundance of *Dorea* species increases after fermentation of the human fecal microbiota on FOS (18). *Dorea longicatena* is stimulated in mouse fecal microbiota after mice were transplanted with a human microbiota and fed FOS (19). Furthermore, we previously demonstrated that many prominent uncultured human gut bacteria, of which the benefits or risks for human health are not known, are well equipped to metabolize prebiotics, including FOS (20). Besides, several pathogenic *Escherichia coli* strains, including strain BEN2908 that has the ability to invade human epithelial cells (21), can metabolize FOS (13, 22). In any event, regardless of their microbial origins, there has been little investigation of the mechanisms of FOS metabolization at the molecular level.

In bacteria, the complete metabolization of glycosides requires at least a set of carbohydrate-active enzymes (CAZymes; <http://www.cazy.org/>) (23) and one or more specific transporters (24, 25). This complex catabolic machinery is encoded by genes clustered within the same genomic loci (26, 27), called polysaccharide utilization loci (PULs) for *Bacteroidetes* (28). This name is further extended to Gram-positive bacteria, known as Gram-positive PULs (gpPULs) (29). As with the other glycans, the proposed mechanism of inulin and FOS metabolization requires four steps (30): (i) extracellular hydrolysis of the longest chains, by cell surface-associated inulinases and/or fructosidases, releasing monosaccharides or short oligosaccharides; (ii) internalization of these short compounds by transporters; (iii) final depolymerization of the oligosaccharides by intracellular fructosidases; and (iv) monosaccharide assimilation in the central metabolism. A variety of bacterial inulin-targeting *Bacteroidetes* PULs (31, 32) and gpPULs (33) have been identified in the past few decades, and many inulinases and fructosidases have been biochemically characterized (34). However, only a few transporters have been proven to internalize FOS: the ATP-binding cassette (ABC) transport systems from the probiotic strain *Lactobacillus acidophilus* NCFM (35) and the oral pathogenic strain *Streptococcus pneumoniae* TIGR4 (36), the major facilitator superfamily (MFS) transporter from the extraintestinal pathogenic *Escherichia coli* strain BEN2908 (22), and two phosphotransferase systems (PTSs) from the probiotic strain *Lactobacillus plantarum* ST-III (37). Nevertheless, the binding and transport specificity of these transporters have still not been determined.

There are, in fact, several technological barriers to the functional characterization of transporters in native bacteria. Despite major advances for some bacterial genera over the last 10 years (38, 39), the difficulties of genetic manipulation, often combined with functional redundancy, render it challenging to characterize transport systems. In the case of uncultured species, it is impossible to inactivate or delete genes. Notably, these species make up more than 70% of the human gut ecosystem (40). In addition, transmembrane proteins cannot be studied as easily as soluble proteins. Consequently,

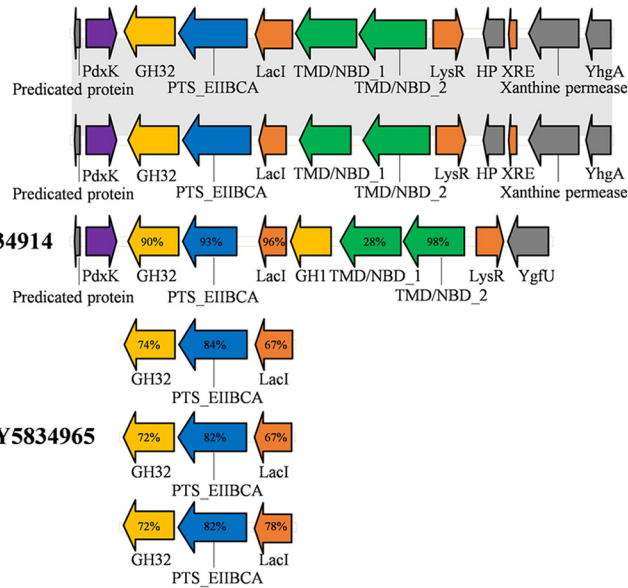
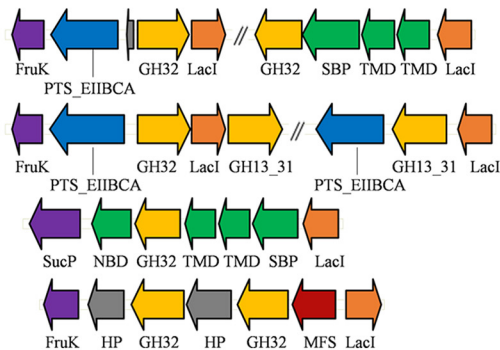
experimental validation of function has taken place for only a few glycoside transporters, while there are probably hundreds of thousands in bacteria, considering that the PUL database lists more than 30,000 *Bacteroidetes* sequences for the SusC/D transporter family alone from 1,154 species (28).

Here, we present a highly generic approach to *in vitro* and *in cellulo* characterization of the binding and transport specificities of membrane-bound proteins based on heterologous expression in *E. coli*. Our strategy combines PUL engineering, analysis of growth dynamics, characterization of transporter functionality, and quantification of binding and transport rates. This novel strategy allowed us to deeply characterize a FOS PTS transporter issued from a dominant uncultured *Dorea* strain, previously identified by mining the human ileal microbiome for prebiotic metabolization pathways (20). This *Dorea* FOS utilization system is the first prebiotic metabolization pathway to be characterized from a nonbeneficial human gut bacterium.

## RESULTS

**Organization of the *Dorea* FOS utilization locus.** By means of activity-based screening of the human ileal metagenome, we previously identified a fosmid *E. coli* clone (clone I9) producing intracellular fructosidase activity responsible for the hydrolysis of a mixture of FOS, containing 1-kestose (GF<sub>2</sub>), nystose (GF<sub>3</sub>), and 1<sup>F</sup>-fructofuranosyl-nystose (GF<sub>4</sub>) (20). After sequencing the I9 metagenomic DNA, two contigs were obtained, I9a and I9b, with sizes of 14,714 and 13,700 bp, respectively. The I9a contig encodes a FOS utilization locus, containing genes annotated as encoding a glycoside hydrolase belonging to the family GH32 of the CAZy classification, a PTS component, a transcriptional regulator of the Lacl family, and two ABC transporter proteins (Fig. 1a). No peptide signal was identified in the GH32 sequence, indicating a cytoplasmic location of this enzyme in the native organism. The RPS-BLAST analysis against the NCBI's conserved domain database (CDD) indicated that both proteins annotated as ABC transporters are multidomain proteins, each with a transmembrane domain (TMD) and a cytosolic nucleotide-binding domain (NBD), which together constitute a complete ABC transporter that nevertheless lacks a solute binding protein (SBP). The same bioinformatic analysis of the PTS transporter sequence of the I9a contig was performed. PTSs are multiple-component carbohydrate uptake systems, allowing the phosphoryl group from phosphoenolpyruvate (PEP) to be successively transferred from enzyme I (EI) to the histidine protein (HPr), then to the domains A and B of enzyme II (EII), and finally to the carbohydrate bound to the EII C domain (41). The I9 PTS sequence analysis revealed that it is a single multidomain protein, composed of the three domains B, C, and A of the PTS EII complex. We thus named it PTS\_EIIBCA. The I9 FOS utilization locus lacks genes encoding EI and HPr. As EI and HPr have been proven to be nonspecific and shared by different PTS systems (42, 43), we hypothesized that *E. coli* EI and HPr could complement the I9 PTS\_EIIBCA. Moreover, no transmembrane helix was predicted in the EIIA and EIIB domains, but ten were found in the EIIC domain, suggesting that the EIIC domain is membrane spanning and could potentially bind extracellular substrates.

The I9a nucleic acid sequence presents 99% identity on 93% of its length with a part of the *Dorea longicatena* DSM 13814 genome (Fig. 1a). In addition, the I9a sequence presents a microsynteny, covering the GH32- to the Lacl-encoding genes, with several human gut *Firmicutes* genomes, such as *Dorea longicatena*, *Ruminococcus torques*, and *Coproccoccus* sp., which all belong to the *Clostridiales* order (Fig. 1a). To date, no FOS utilization locus has been characterized from *Clostridiales*, even though several species in this order have been proven to metabolize FOS *in vitro* (13, 44). In contrast, several other *Firmicutes* loci harboring just one of the PTS or ABC transport systems associated with at least one GH32 and a regulator have been proposed to be involved in the utilization of FOS by *Lactobacillus* spp. using transcriptomic analysis, sometimes combined with gene inactivation (Fig. 1b) (35, 37, 45). In *Streptococcus pneumoniae*, two GH32-containing loci, the *scr* locus including a PTS transporter and the *sus* locus including an ABC transport system, were shown to be responsible for the utilization of sucrose and FOS, respectively (Fig. 1b) (36). Here, though, we observed both transport

**a****I9 metagenomic locus****b****Streptococcus pneumoniae TIGR4****Lactobacillus plantarum ST-III****Lactobacillus acidophilus NCFM****Escherichia coli BEN2908**

**FIG 1** Representations of FOS and sucrose utilization loci. (a) Alignment of the I9 metagenomic FOS utilization locus with similar loci from cultured bacteria. Synteny between the I9 sequence and the genomic locus of *D. longicatena* DSM 13814 is shown by gray bars. Percentages of identity are indicated when lower than 100%. (b) Alignment of the characterized FOS and sucrose utilization loci involving either an ABC, an MFS, or a PTS transport system, a GH32, and a related regulator. Genes predicted as being involved in carbohydrate sensing, transport, and hydrolysis are color coded: glycoside hydrolases (GH) in yellow, PTS in blue, ABC transporter components in green (NBD, nucleotide binding domain; TMD, transmembrane domain; SBP, solute binding protein), MFS in red, LacI regulator and XRE (xenobiotic response element) family transcriptional regulator in orange, and PdxK (pyridoxine kinase), FruK (fructokinase), and SucP (sucrose phosphorylase) in purple. The other genes are indicated in gray: hypothetical protein (HP), xanthine permease, YhgA (putative YhgA-like transposase), and YgfU (putative purine permease).

systems localized in the same locus. The presence within the same locus of both transport systems suggests a difference in the specificities of the I9 ABC and PTS.

#### Abundance of the *Dorea* FOS utilization locus in the human gut microbiome.

The prevalence and abundance of the genes within the *Dorea* FOS utilization locus in the human gut microbiome were quantified from the abundance table of the human gut metagenomic gene catalogue (Fig. 2) built from fecal samples from 1,267 individuals of various geographic origins (America, Europe, and China), lifestyles, and medical statuses (46).

We found that eight genes of the I9 locus have homologs (with more than 97% sequence identity and 100% coverage) in the microbiome. These genes are highly prevalent, being present in at least 50% of the individuals in the cohort. Interestingly, the *pts\_EIIBCA* gene is 4.6 times less abundant than the other genes of the locus, although with a similar prevalence. This result indicates that the structure of the *Dorea* FOS locus has been altered during its evolution, which might be due to (i) the a





**FIG 2** 19 FOS utilization locus abundance and prevalence in the human gut microbiome. Gene abundance in the fecal metagenome is represented by a color scale: white, not detected; blue, turquoise, green, yellow, orange, and red, increasing abundance with a 10-fold change between colors. Based on its annotation, the xanthine permease-encoding gene is not involved in carbohydrate binding, sensing, transport, or modification.

*posteriori* gene acquisition of the *Dorea pts* gene from an existing locus or (ii) its loss within some bacterial populations over time. Both events could have been driven by horizontal gene transfer, an essential phenomenon for bacterial genome plasticity and metabolic adaptability (47). Nevertheless, when comparing gene abundance and prevalence in the microbiome of individuals of various origins and medical statuses, the *pts* gene presents the same relative profile as the other genes of the FOS utilization locus. The six genes are indeed on average 3 and 6.5 times more prevalent and abundant, respectively, in Westerners (including Americans and Europeans) than in individuals of Chinese origin. This is probably due to the dietary differences between Westerners and Asians. Wheat is a major source of FOS (5), and bread made with wheat is a staple food for Westerners (48, 49), while for Asians, it is rice (50, 51).

In addition, in the European cohort, these genes are similarly prevalent but twice as abundant in the microbiomes of patients suffering from inflammatory bowel diseases (IBDs; including Crohn's disease and ulcerative colitis) than in those of healthy individuals. This suggests that bacteria possessing this FOS utilization locus may be positively associated with IBD.

#### The *Dorea* phosphotransferase system confers FOS utilization ability to *E. coli*.

First, in order to identify which genes expressed in *E. coli* could explain the *Dorea* 19 FOS utilization phenotype, the gene expression levels were quantified by reverse transcription-quantitative PCR (RT-qPCR) for the four genes potentially involved in substrate internalization (*pts\_EIIBCA*, *tmb/nbd\_1*, and *tmb/nbd\_2*) and hydrolysis (*gh32*) (see Fig. S1 in the supplemental material). Except for *tmb/nbd\_2*, which displayed a relatively low expression, all the genes were expressed at increased levels compared to that of the endogenous *E. coli* housekeeping gene (*ihfB*). The moderate expression of the ABC transporter-encoding genes suggests that the ability of *E. coli* to internalize FOS might be mostly due to the expression of the *pts\_EIIBCA* gene. In addition, this transcriptomic study highlights the potential of *E. coli* to properly express *Firmicutes* genes cloned in fosmids. This result is consistent with our previous study performed with a *Bacteroidetes* PUL, demonstrating that a significant proportion of metagenomic genes could be expressed spuriously in *E. coli* due to the presence within the metagenomic sequence of numerous  $\sigma^{70}$  promoter sequences for *E. coli* (52).

Second, in order to establish the contribution of each gene in the *Dorea* FOS locus in the ability of *E. coli* to metabolize FOS, different truncated variants of the 19

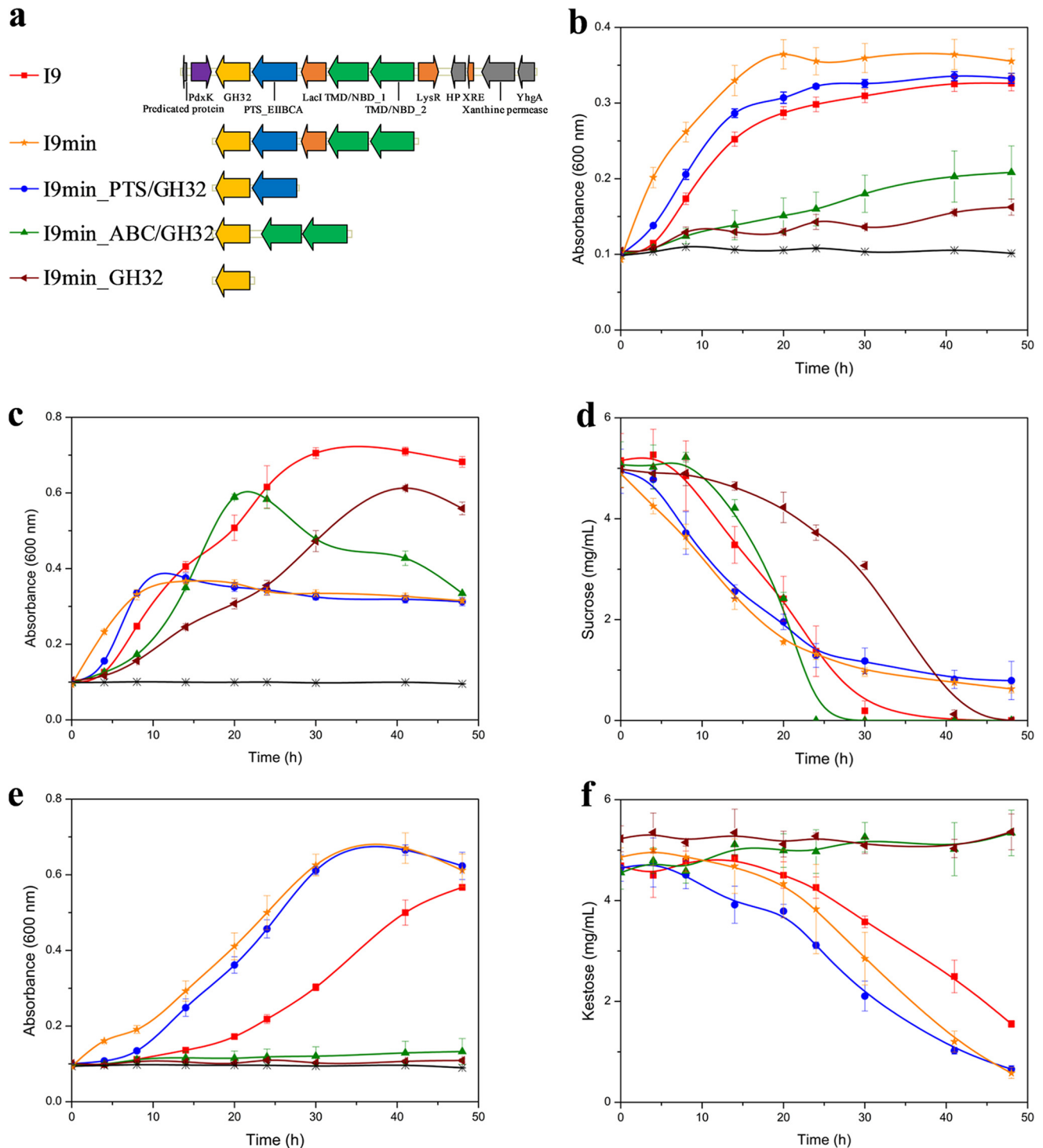


**FIG 3** Functional analysis of the I9 FOS utilization locus. (a) Gene organization in the I9 variants. Growth curves of clone I9, its variants, and the control clone EPI on FOS mixture (b), sucrose (c), and kestose (e). HPAEC-PAD analysis of the culture supernatants for growth on sucrose (d) and kestose (f). Color code: clone I9, red; I9min, yellow; I9min\_PTS/GH32, blue; I9min\_ABC/GH32, green; I9min\_GH32, brown; EPI, black. The symbols indicate the sampling time points. The data represent the averages from biological triplicates.

metagenomic DNA insert were generated (Fig. 3a). The *E. coli* host transformed with the empty fosmid pCC1FOS, here named EPI, was used as a negative-control strain.

We showed that only the I9 GH32 enzyme was responsible for FOS hydrolysis by testing cytoplasmic cell extracts of the I9 variant harboring only the GH32 (I9min\_GH32)

on pure sucrose, kestose, nystose, fructosyl-nystose, inulotriose, inulin, and levan. Among these carbohydrates, only sucrose, kestose, nystose, fructosyl-nystose, and inulotriose were hydrolyzed (Fig. S2; see also Table S2 in the supplemental material). Moreover, this enzyme prefers sucrose and FOS up to degree of polymerization 4 (DP4) to longer oligosaccharides, since fructosyl-nystose was not fully hydrolyzed and even present at a lower molar concentration than nystose and kestose (Table S2). In contrast, EPI cytoplasmic extracts displayed no activity on the same substrates, validating the fact that the *E. coli* EPI100 host strain was not able to hydrolyze FOS. In addition, no secreted activity was detected in I9min\_GH32 (data not shown), confirming that the GH32 enzyme is produced exclusively inside the *E. coli* cells.

To determine the internalization specificity of the two I9 transporters (the PTS and the ABC transport system), the ability of truncated variants to use FOS as the sole carbon source was assessed (Fig. 3b). First, by constructing an I9-reduced variant consisting of the genes from *gh32* to *tmb/ncd\_2* (I9min), we confirmed that only this minimal locus was responsible for the growth on FOS. The I9 and I9min clones in fact displayed similar growth on FOS. The slight difference might result from the high number of recombinant proteins that have to be produced in I9, which slowed down its growth compared to that of I9min. Interestingly, the clone I9min\_GH32 grew slowly on the FOS mixture. This result indicates that the EPI100 host strain possesses at least one nonspecific transporter able to internalize at least one of the components of the FOS mixture that is further metabolized by the host after hydrolysis by the intracellular GH32. The I9min\_PTS/GH32 variant, harboring the PTS transporter and the GH32, retained the growth ability of I9 on FOS. In contrast, the growth of I9min\_ABC/GH32 on FOS was strongly impaired, with a growth rate barely higher than that of I9min\_GH32. The modest growth of I9min\_ABC/GH32 might be due to the uptake of sucrose from the FOS mixture, but at this stage of the study, we could not exclude that the ABC transporter has a very low ability to transport FOS.

To characterize the transport specificity of each I9 transport system more precisely, for each variant, we monitored the consumption of individual FOS components in the culture medium using high-pH anion-exchange chromatography-pulsed amperometric detection (HPAEC-PAD) (see Fig. S3). First, as proposed above, the host strain EPI100 possesses its own sucrose transporter, since the amount of sucrose slightly decreased over time for I9min\_GH32. When growing on the FOS mixture, clones I9, I9min, and I9min\_PTS/GH32 preferentially metabolized sucrose (GF) and kestose (GF<sub>2</sub>), while nystose (GF<sub>3</sub>) and 1<sup>F</sup>-fructofuranosyl-nystose (GF<sub>4</sub>) were not used. In contrast, I9min\_ABC/GH32 consumed only sucrose. No increase in the oligosaccharide concentration was observed in the culture medium during growth, indicating that the I9 ABC and PTS transporters are both importers, contrary to what was observed with similar analyses for other transport systems, such as those from the major facilitator superfamily (MFS) (52). To confirm the specificity of the transporters either for sucrose or kestose, the uptake of these two oligosaccharides was examined by growth test and HPAEC-PAD analyses (Fig. 3c to e and f). All the variants were able to use sucrose to grow except EPI. However, sucrose appears not be the favorite substrate for the PTS transporter, as the growth rate of I9min\_PTS/GH32 on sucrose was lower than for I9. I9min\_ABC/GH32 grew more rapidly than I9min\_GH32 on sucrose, but these PTS-devoid clones were unable to use kestose. This demonstrates that even if the host strain possesses its own sucrose transporter, the I9 ABC transporter has the ability to transport sucrose. As far as we know, it is the first example of carbohydrate importer of the ABC transporter family which lacks an SBP (53). When the SBP is lacking, such as in ABC transporters catalyzing micronutrient uptake (54), the TMDs determine the specificity of the transporter through substrate-binding sites. Nevertheless, the mechanism explaining how the I9 ABC transporter could import sucrose without SBP remains to be characterized.

To deeper analyze the specificity of the PTS and ABC transporters to fructans and fructooligosaccharides, the growth of I9 was also tested on inulin (GF<sub>n</sub> with  $\beta$ -1,2-linked fructosyl units), levan (GF<sub>n</sub> with  $\beta$ -2,6-linked fructosyl units), and inulotriose (F3 with  $\beta$ -1,2-linked fructosyl units). No growth was observed with any of these carbohydrates



(data not shown). However, we found that the GH32 enzyme was able to hydrolyze inulotriose *in vitro* (see Fig. S2b and Table S2), demonstrating that the metabolism of inulotriose by I9 is blocked at the transport step. From these results, we conclude that (i) the I9 PTS is specific to sucrose and kestose (with a clear preference for kestose) and requires a terminal glucosyl moiety to recognize the oligosaccharide to be internalized and (ii) the I9 ABC transporter is able to transport sucrose only.

**Binding specificity of the *Dorea* PTS transporter.** To determine the transport and binding specificities of the PTS transporter, we had to establish a new methodology. Up until now, the characterization of transporter specificity, performed *in vivo* by growth analysis after knockout (55), the determination of the internalization rate of radiolabeled substrates (56), and/or transcriptional analysis (57), did not allow for separate analyses of the binding, transport, and metabolism specificities. In addition, the substrate of transcription activation differs from the substrate that is transported (58). Binding specificity can be determined *in vitro* by characterizing purified binding proteins by isothermal calorimetry, affinity gel electrophoresis (59), thermal shift assay in the presence of substrates to identify their impact on protein stability, pulldown analysis on beads covalently linked to the different sugars (60), or a scintillation proximity assay with radiolabeled substrates (61). However, protein purification can be challenging, especially for membrane-bound proteins (such as I9 PTS\_EIIBCA). Moreover, in all the previous studies aiming to characterize binding specificity, the binding protein is dissociated from the multiprotein assembly, which could potentially bias the results of specificity determination.

Here, we developed an easy-to-implement method based on the use of crude extracts of the cells harboring the target transporter and nonlabeled natural substrates. The unbound amounts of these are quantified by HPAEC coupled to PAD, a highly sensitive detection method. This generic approach can be used to quantitatively analyze the specificity of any transporter. We established the proof of concept by characterizing the *Dorea* PTS produced in *E. coli*. A truncated variant of I9, consisting only of the PTS (named I9min\_PTS), was constructed in order to avoid any bias due to oligosaccharide hydrolysis in oligosaccharide uptake rate quantification. First, the uptake assays were performed with intact I9min\_PTS cells incubated with various oligosaccharides in order to determine the PTS ability to internalize substrate (Fig. 4a). Using HPAEC-PAD, the amount of residual substrate was measured in the supernatant at different time points. We observed that among the different gluco- and fructooligosaccharides tested (kestose, nystose, fructosyl-nystose, inulotriose, and celotriose), only kestose decreased in amount after incubation with I9min\_PTS, confirming that the *Dorea* FOS PTS was specific to kestose. However, by incubating intact cells with the substrate, we could not determine the contribution of binding in the uptake process.

The ability of membrane debris to bind substrate was thus determined by incubating I9min\_PTS lysed cells with oligosaccharides. To focus only on the binding step, cell debris was washed several times before the incubation to eliminate *E. coli* cytoplasmic phosphate, HPr, and EI in the reaction mixture, as this could lead to substrate phosphorylation and bias in binding rate quantification. As with the uptake assays, only kestose was bound by the I9min\_PTS membranes (Fig. 4a). The PTS\_EIIBCA was more slowly saturated by kestose with membrane extracts than with intact cells (Fig. 4b), indicating that kestose internalization shifts the binding equilibrium. Such a low rate of translocation had already been observed with the diacetylchitobiose-specific PTS from *Vibrio furnissii* 7225, where the transport kinetic was characterized by incubating growing *V. furnissii* cells on radiolabeled diacetylchitobiose (62). The low rate of this internalization process might be due to the covalent modification of substrate, in contrast to what happens with ABC transporters which hydrolyze ATP (54) or with secondary transporters such as the MFS, which use a chemiosmotic ion gradient to accelerate uptake (63).

Carbohydrate binding to the transporter is the first and essential step in an active transport system. The ligand-protein binding kinetic is fundamentally related to trans-

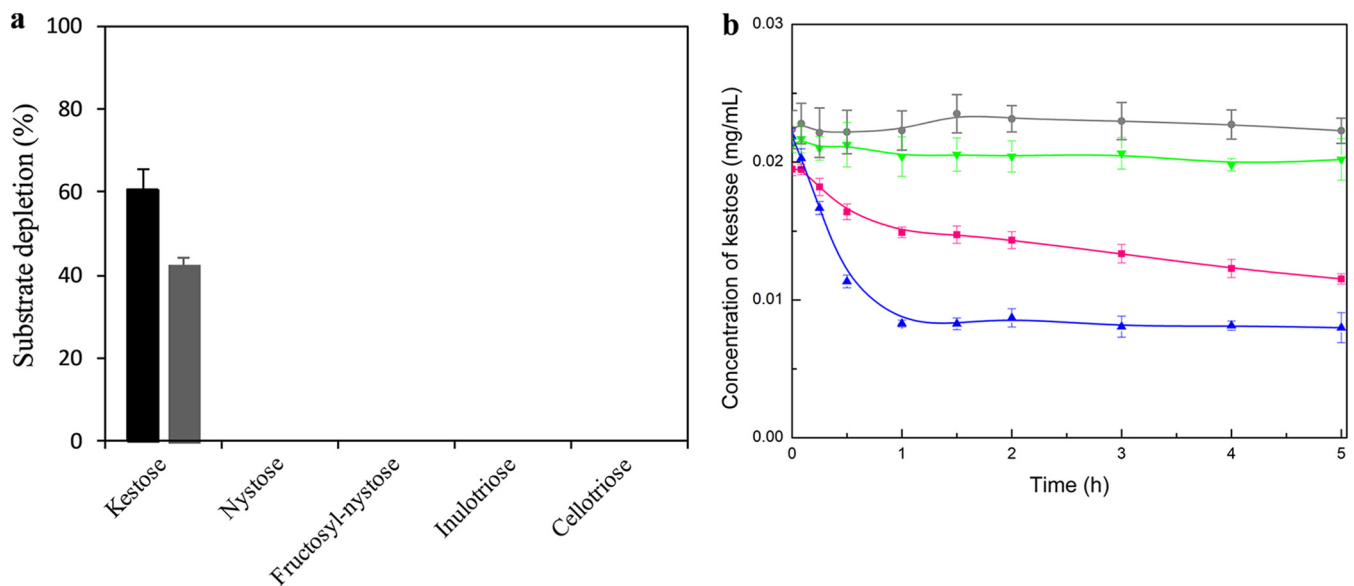


**FIG 4** Oligosaccharide uptake and binding by I9min\_PTS cells. (a) Screening of PTS specificity by testing the binding (gray bar) and uptake (black bar) of various gluco- and fructooligosaccharides by I9min\_PTS cells. Oligosaccharide concentration was determined by HPAEC-PAD after 1 h of incubation of the oligosaccharides with I9min\_PTS crude membrane cell extracts (for binding) or intact cells (for uptake). (b) Kestose binding and uptake kinetics by I9min\_PTS crude membrane cell extracts and intact cells, respectively. Kestose concentration in the soluble phase was determined by HPAEC-PAD; EPI cells in green, EPI membrane extracts in gray, I9min\_PTS cells in blue, and I9min\_PTS membrane extracts in pink. The data represent the means from three biological replicates.

port efficiency and microbial chemotaxis in ecological niches (64, 65). Here, we determined reliable kinetic parameters for binding, transport, and growth of I9 PTS to kestose (Fig. 5). Saturation experiments were performed on I9min\_PTS cells and their membranes with increasing concentrations of kestose. The affinity constants of kestose uptake by I9min\_PTS cells ( $K_m$ ) and of kestose binding by PTS\_EIIBCA membranes (dissociation constant [ $K_d$ ]) were  $266 \pm 165$  and  $51 \pm 12 \mu\text{M}$ , respectively. Even if these values are of the same order of magnitude, the fact that the  $K_m$  value is higher than the  $K_d$  one indicates that uptake is slightly less efficient than binding. It might be due to the complexity of the translocation process, which involves three PTS subunits (EIIC, EIIA, and EIIB), against only one (the EIIC part that faces the exterior of the cell) for binding. In addition, to infer the dependence of growth rate on kestose concentration, we estimated the substrate affinity constant ( $K_s$ ) by applying the Monod model (e.g., Michaelis-Menten hyperbolic dependence) to the growth rate of the I9min\_PTS/GH32 cells versus kestose concentration data (66). The estimated  $K_s$  value of  $5.68 \pm 0.77 \text{ mM}$  differs by 2 orders of magnitude from the uptake and binding constants. These kinetic binding parameters indicate that the I9min\_PTS/GH32 strain has a strong binding affinity and efficient uptake system for kestose but a poor capacity to metabolize it. In the human gut, this kind of high-affinity uptake system is crucial for competing with other microbes for limited amounts of kestose. Furthermore, the inconsistency between the values of  $K_s$ ,  $K_d$ , and  $K_m$  shows that kinetic data for growth cannot be used to predict transporter binding and internalization ability.

**Functionality of the *Dorea* PTS transporter in *E. coli*.** PTS transporters couple transmembrane transport of substrate to its concomitant phosphorylation. However, the ability of PTS to phosphorylate a trisaccharide has never been shown until now. To demonstrate the full functionality of *Dorea* PTS\_EIIBCA in *E. coli* and to identify the potential transient presence of intracellular phosphorylated kestose, we analyzed the intracellular metabolites of clone I9min\_PTS/GH32 grown on kestose by ion chromatography coupled with electrospray ion ionization high-resolution mass spectrometry (IC-ESI-HRMS) (67) after quenching the metabolism (Fig. 6a).

As the *E. coli* without I9 PTS\_EIIBCA did not grow on kestose, it could not be used as negative control. We thus compared the results obtained on kestose with those

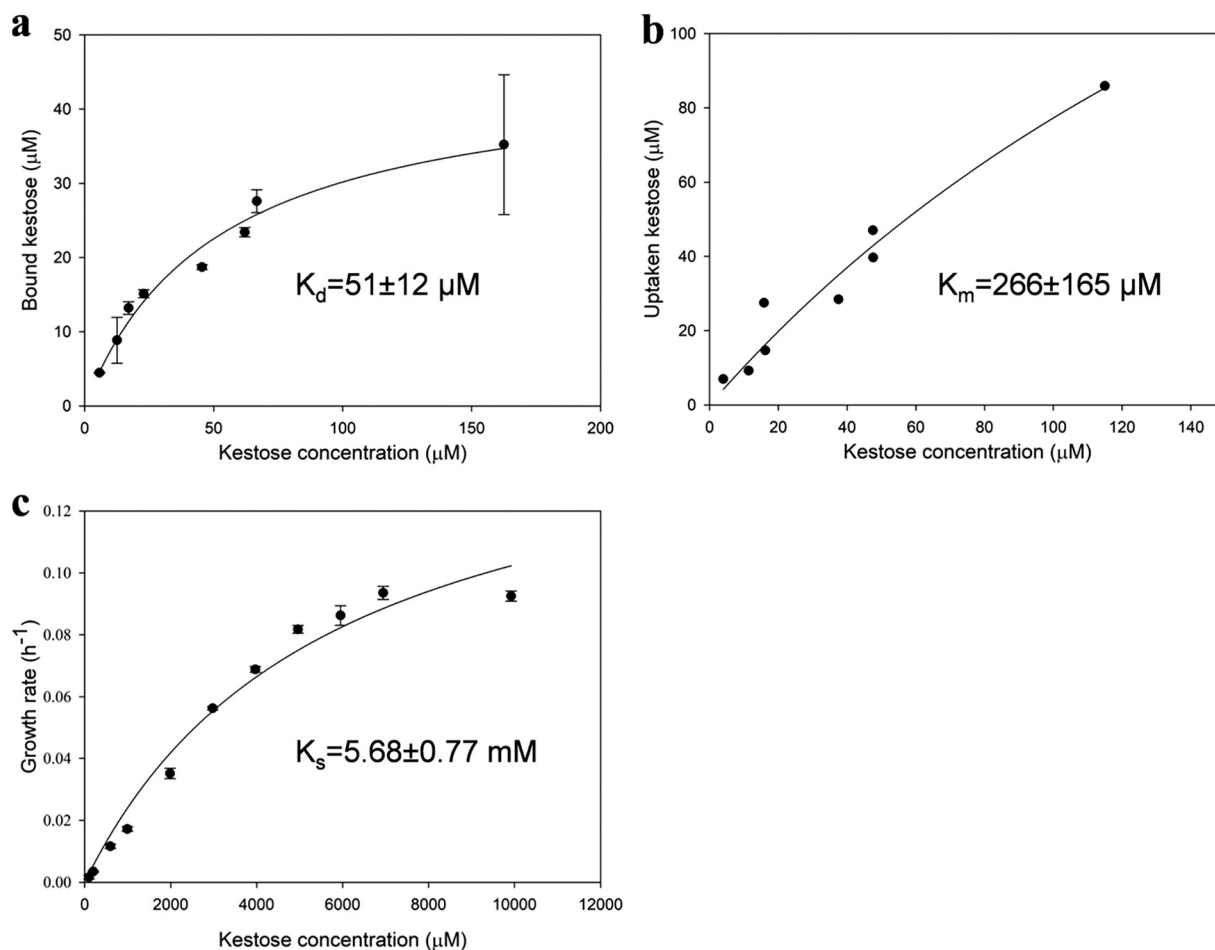


**FIG 5** Saturation experiments on the *Dorea* PTS. Binding saturation of PTS\_EIIBCA in I9min\_PTS membranes (a), uptake saturation of I9min\_PTS cells (b), and growth saturation of I9min\_PTS/GH32 (c) with increasing concentrations of kestose. The data represent the means from two biological replicates.

obtained with clones I9min\_PTS/GH32 and of the KEIO collection (68) transformed with the empty fosmid pCC1FOS grown on glucose. For all strains, we searched for an  $m/z$  value of 583.1270, which corresponds to the theoretically expected value in negative mode for the phosphorylated kestose. For the I9min\_PTS/GH32 and EPI strains grown on glucose, the extracted ion chromatogram (XIC) does not show any peak. In contrast, we detected a chromatographically unresolved peak at retention time of 13.17 min for the I9min\_PTS/GH32 strain grown on kestose (Fig. 6a), indicating the presence of several different forms of phosphorylated kestose.

Based on the above-described results, the I9 PTS\_EIIBCA harboring the three well known domains of PTS transporters (A, B, and C domains) appears to be responsible for kestose internalization and phosphorylation by *E. coli*. As explained above, phosphorylation requires a multiproteic machinery to transfer the phosphoryl group from intracellular PEP to the carbohydrate bound to the EIIc domain of the PTS (41). Because the I9 locus lacks the EI and HPr components of the PTS (while being present elsewhere in the genome of *Dorea longicatena* DSM 13814, with the EI and HPr conserved histidine residues required for phosphate transfer), we hypothesized that the *E. coli* PTS machinery could complement I9 PTS\_EIIBCA to achieve kestose phosphorylation. To investigate this question, we verified the ability of *E. coli* K-12 BW25113 (KEIO collection strains) single-knockout mutants for glucose and fructose-specific PTS genes transformed with fosmid I9min\_PTS/GH32 to grow on a mixture of FOS, from which only kestose is utilized, as demonstrated above in the present paper. The *ptsI* (encoding EI)

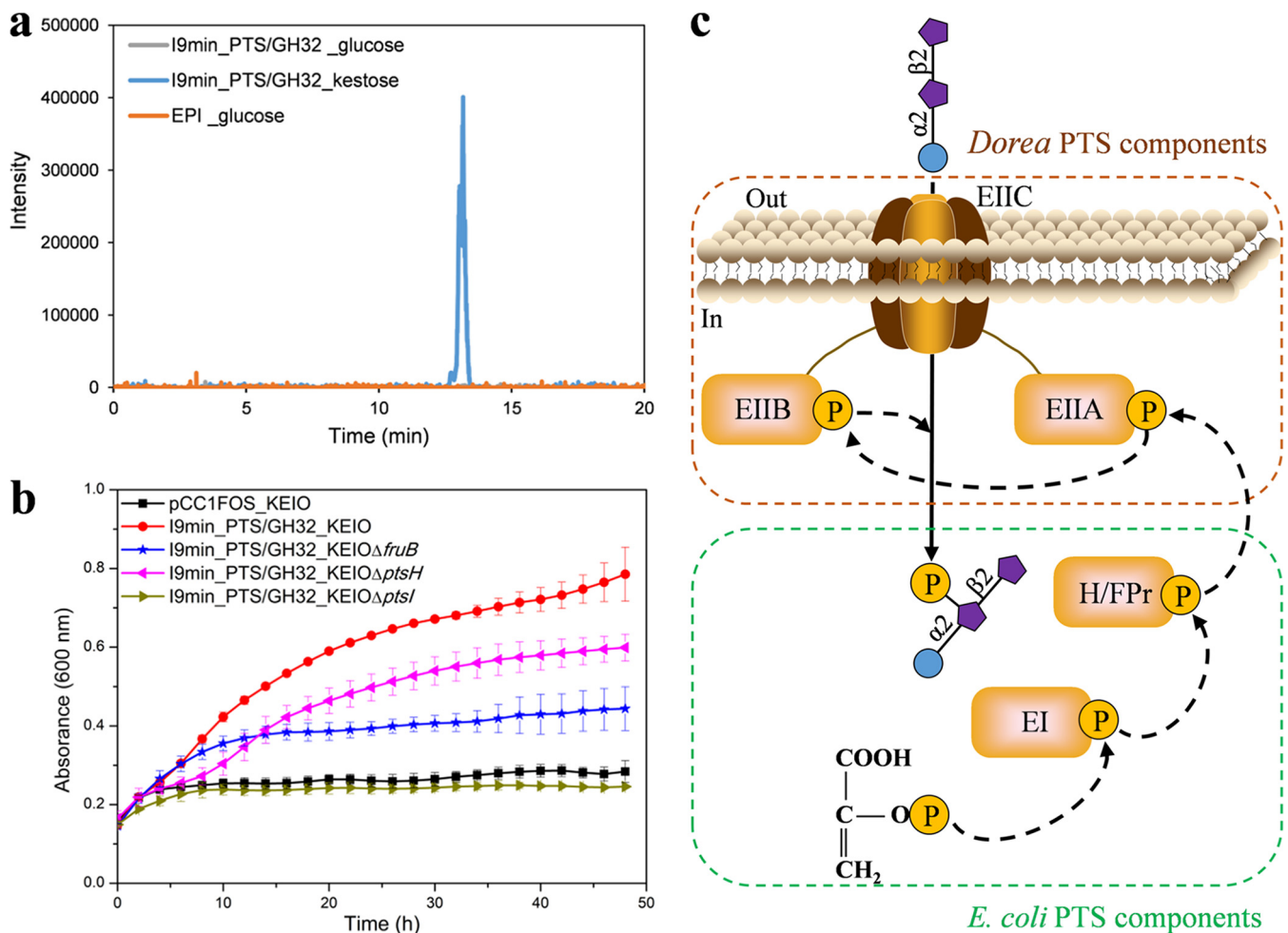


**FIG 6** Functionality of the *Dorea* PTS in *E. coli*. (a) Extracted ion chromatogram (XIC) from negative ionization mode analysis at  $m/z$  583.1270, corresponding to the exact mass of the  $[M-H]^-$  ion of phosphorylated kestose (calculated from the molecular formula  $C_{18}H_{33}O_{19}P$ ). Color code: I9min\_PTS/GH32 clone grown on kestose, blue line; I9min\_PTS/GH32 grown on glucose, gray line; EPI grown on glucose, orange line. (b) Growth curves on FOS of *E. coli* K-12 BW25113 (KEIO) single-knockout mutants for PTS genes (*ptsI*, *ptsH*, and *fruB*) transformed with fosmid I9min\_PTS/GH32. The KEIO wild-type strain transformed with the empty fosmid pCC1FOS was used as the negative control. HPr (histidine protein) encoded by *ptsH* is a cytoplasmic protein component of the *E. coli* glucose PTS. It accepts a phosphate group from EI (encoded by *ptsI*), a cytoplasmic protein required for *E. coli* PTS functioning, and transfers it to the carbohydrate-specific EIIA domain. *fruB* encodes the HPr-like component FPr of the *E. coli* fructose PTS. These data represent the means from three biological replicates. (c) Schematic representation of 1-kestose transport and phosphorylation by the *Dorea* PTS complemented with the *E. coli* HPr, FPr, and EI component. As shown in panel a, kestose can be phosphorylated at different carbon positions, while only one form of phosphorylated kestose is represented here.

defective strain was unable to utilize FOS as carbon sources (Fig. 6b), demonstrating that this *E. coli* enzyme is required to ensure FOS-PTS functionality. Indeed, EI is involved in the first step of phosphorylation from PEP, which explains why deletion of *ptsI* in the KEIO strain completely abolished its growth on glucose and fructose (see Fig. S4). In contrast, mutants defective for *ptsH* (encoding histidine protein HPr, which transfers the phosphate group from EI to the EIIA component of the glucose PTS) or *fruB* (encoding HPr-like FPr in the fructose PTS) were able to grow on FOS, even though their growth ability was reduced compared to that of the wild-type strain transformed with I9min\_PTS/GH32 (Fig. 6b). Similarly, deletion of *ptsH* or *fruB* in the KEIO strain resulted in a delayed lag phase when grown on glucose or fructose, respectively (Fig. S4), indicating that HPr could compensate for FPr deficiency and vice versa. We thus conclude that *Dorea* PTS\_EIIBCA requires the *E. coli* EI to transfer phosphate from PEP to *E. coli* HPr (which can also be replaced, less effectively, by FPr), which, in turn, phosphorylates the I9 EIIA domain. Phosphate is then transferred to the I9 EIIB domain and, ultimately, to the kestose molecules internalized through the I9 EIIIC component (Fig. 6c).

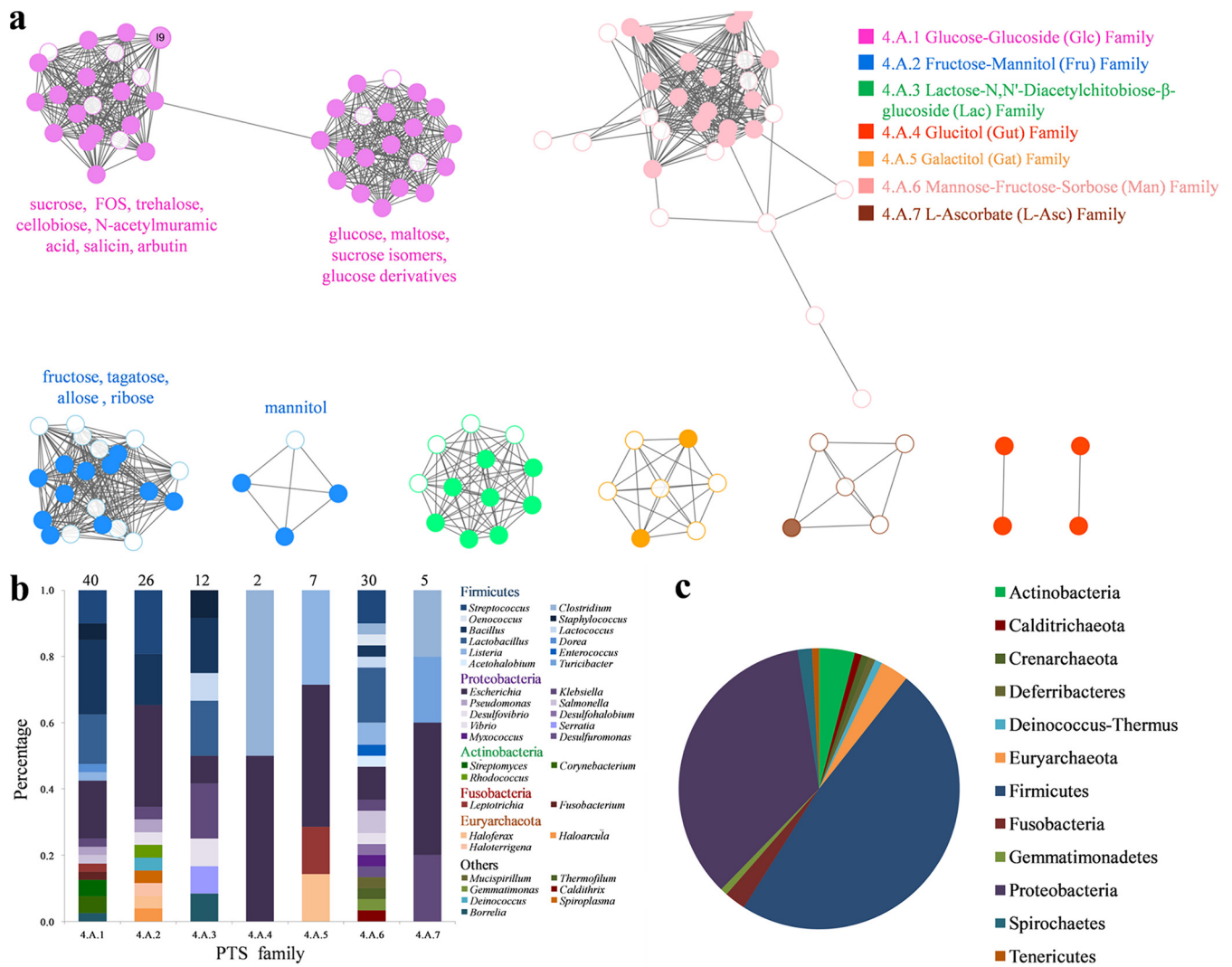


**FIG 7** Functional, structural, and taxonomical diversity of PTS. (a) Sequence similarity network (SSN) of PTS-EIIC domains from 125 proteins, retrieved from the Transporter Classification database, from the literature, and from the present study, constructed with an initial score of  $10^{-5}$ . The nodes are connected by an edge if the pairwise sequence identity is  $\geq 21.3\%$ . The corresponding substrates were annotated under each cluster of the 4.A.1 and 4.A.2 families. Unfilled nodes indicate sequences for which the functions were inferred by transcriptomics, while filled ones correspond to the functions validated biochemically or by gene deletion. Taxonomic distributions at genus (b) and phylum (c) levels of the characterized PTS transporters.

**PTS structural, functional, and taxonomical diversity.** By analyzing the specificity of *Dorea* PTS\_EIIBCA, we extended the panel of characterized glycoside transporters, which is still limited. Prior to this study, only two PTSs (PTS1 and PTS26 from *L. plantarum* ST-III) were known to internalize FOS (37). However, these proteins are not listed in the Transporter Classification database (TCDB) (69). In the TCDB, based on functional and phylogenetic information about the EIIC domain (as in the first classification of PTS proposed by Nguyen et al. [70]), PTSs have been classified into seven families of phosphotransfer-driven group translocators, consisting of the glucose-glucoside (4.A.1, Glc), fructose-mannitol (4.A.2, Fru), lactose-*N,N*-diacetylchitobiose (4.A.3, Lac), glucitol (4.A.4, Gut), galactitol (4.A.5, Gat), mannose-fructose-sorbose (4.A.6, Man), and L-ascorbate (4.A.7, L-Asc) families.

To locate the FOS transporters in the diversity of PTSs and to investigate the sequence-function relationships of these proteins, we constructed a sequence similarity network (SSN) from the 125 sequences of EIIC components retrieved from TCDB (120 sequences for 117 PTSs, since 3 have 2 EIIC domains), the literature (4 sequences), and the present study (Fig. 7a). In an SSN network, nodes (representing protein sequences)



in the same cluster are connected with an edge if they share a percentage of identity higher than a threshold value, providing a more visually tractable view of divergent proteins than alignment-based dendrograms or phylogenetic trees (44). First, despite the low sequence identity threshold used to link the nodes in the sequence network to form clusters (21%), we observed that the 3 FOS PTSs (one from *Dorea* and two others from *L. plantarum* DT-III) do not belong to the cluster of sequences containing the members of the Fru family 4.A.2. Even though FOSs contain more fructosyl than glucosyl moieties (one terminal glucosyl moiety in a FOS molecule, regardless of its degree of polymerization), the FOS PTSs belong to the Glc family 4.A.1. This could correlate to the fact that the *Dorea* PTS requires the terminal glucosyl moiety of FOS to bind and internalize its substrate.

Second, we observed that the two large Glc and Fru PTS families are subdivided into two clusters each in the SSN. The 4.A.1 Glc family contains two subfamilies in the TCDB, each corresponding to one of the SSN clusters: (i) subfamily 4.A.1.1, named “glucose subfamily” in the TCDB, contains PTSs specific to glucose, its derivatives (such as *N*-acetylglucosamine), and also  $\alpha$ -glucosides such as maltose and sucrose isomers; (ii) subfamily 4.A.1.2, named “glucoside subfamily,” contains PTSs targeting  $\alpha$ - and  $\beta$ -glucosides, such as sucrose (GF), trehalose ( $\alpha$ -1,1-linked GG, which has a close structural similarity to sucrose [71]), FOS (GFn), cellobiose ( $\beta$ -1,4-linked GG), and other  $\beta$ -glucosides (salicin and arbutin), and *N*-acetylmuramic acid. If the present SSN clusters correspond to the TCDB 4.A.1 subfamilies, they are not the same as those previously proposed by Nguyen et al., who categorized the proteins now listed in the 4.A.1 family into the glucose (Glc) and  $\beta$ -glucoside (Bgl) families (70). Regarding the 4.A.2 Fru family, for which no subfamily is described in the TCDB, one SSN cluster contains the transporters targeting fructose, tagatose, ribose and allose, while the other one, clearly separated, contains mannitol-PTS. In this case, this is consistent with the findings of Nguyen et al., who described the mannitol family apart from Fru (70).

From these results, we conclude that there is no longer a link between the names of the families listed in the available PTS classifications and the function of their constituent members. Improvements in transporter classification will be proposed in the following section.

Since phylogenetic links are one of the bases of the existing transporter classifications, we also analyzed the taxonomical diversity of the 125 known PTS\_EIIC sequences. They represent 37 genera, classified into 12 distinct phyla (Fig. 7b and c). For each PTS family, the taxonomic diversity is wide ranging, with no family assigned to a specific phylum or genus. Of 125 sequences, more than half were assigned to the four genera *Escherichia* (20%), *Streptococcus* (10%), *Bacillus* (13%), and *Lactobacillus* (11%). Consequently, more than 80% belong to only two phyla, *Firmicutes* (48%) and *Proteobacteria* (35%). There is a similar distribution of characterized PTSs between Gram-negative and Gram-positive bacteria. The present taxonomic distribution of PTS is highly biased by sequencing and biochemical characterization efforts which are unequal in their coverage of actual bacterial diversity. For example, characterized PTSs are absent from the *Bacteroidetes* phylum, while in the Pfam 32.0 database, we found 10 *Bacteroidetes* sequences harboring a PTS\_EIIC Pfam motif (PF13303) (72). In addition, the characterized PTSs appear to be very abundant in *Firmicutes* (48%) (Fig. 7c), while this phylum accounts for just 29% of the sequenced bacterial genomes (versus 54% for *Proteobacteria*) referenced in the Genomes Online database (GOLD) (73). In any event, though, there are still many transporters to be discovered in the near future thanks to powerful tools such as functional metagenomics and novel generic biochemical approaches, such as those described here.

## DISCUSSION

**Biochemical characterization of a FOS-specific PTS transporter.** The PTS is a multiple component carbohydrate transport and phosphorylation system composed of two cytoplasmic phosphotransferases, enzyme I (EI) and histidine-containing phosphocarrier protein (HPr), which are common in most systems, and one multiproteic enzyme

II complex (EII) including two phosphotransferase proteins (EIIA and EIIB) and one integral membrane protein (EIIC), which is usually specific for one substrate or a small group of closely related carbohydrates. For example, 21 different EII complexes were identified in *E. coli* as being involved in the transport of approximately 20 different carbohydrates, with only 1 EI and 1 HPr protein, and five EI and six HPr paralogues, whose functions are still to be uncovered (43). PTSs are thus major carbohydrate transport systems in certain bacteria, but their diversity and functionalities have been insufficiently investigated. Today, we have just 122 PTSs characterized (either biochemically or by transcriptomics and/or gene deletion), targeting a substrate range (mainly monosaccharides and some glucosides, *N*-acetyl-glucosides, fructosides, and galactosides) that is highly restricted compared to the possible diversity of oligosaccharides (74).

In the present study, we characterized a PTS\_EIIBCA complex involved in FOS utilization by both uncultured and cultured *Dorea* strains. Previously, several FOS PTSs have been identified from lactic acid bacteria and characterized by growth tests and transcriptomic analysis (75, 76), sometimes also with knockout experiments (37), or by measurement of the extracellular composition by anionic exchange chromatography (45). However, the precise molecular mechanism and the exact lengths of the oligosaccharides that could be bound and internalized were not deeply investigated due to the technical bottlenecks inherent in transporter characterization. Here, we developed a highly generic, sensitive, and quantitative method based on HPAEC-PAD analysis of oligosaccharides unbound to crude membranes or to entire cells (native or recombinant). This approach, which requires no protein complex dissociation or purification steps, is compatible with the use of unlabeled natural substrates to quantify binding, transport, and metabolization rates. It thus effectively replaces the use of radiolabeled substrates, which have been widely used until now for transporter characterization. Here, we were able to determine the contributions of substrate binding and transport to the oligosaccharide metabolization process. We proved that *Dorea* PTS\_EIIBCA is able to transport sucrose and especially kestose, with an affinity for kestose binding five times better than its affinity for uptake.

Moreover, carbohydrate uptake through a PTS implies a phosphorylation cascade. PTS-based phosphorylation of oligosaccharides with a DP of more than 2 had never been shown. Here, we proved that a DP3 oligosaccharide can be phosphorylated by *Dorea* PTS\_EIIBCA and that its specificity for phosphorylation is the same as that for binding and translocation. We demonstrated this directly *in cellulo*, in contrast to the previous studies, in which phosphorylation reactions were performed *in vitro* by adding purified phosphotransferases and EIIB to the EIIC component (77). By IC-ESI-HRMS analysis and use of *E. coli* single-knockout mutants, we proved the entire functionality of the *Dorea* PTS\_EIIBCA complex in *E. coli*, thanks to efficient complementation by the host's EI and HPr (or, alternatively, FPr) phosphotransferases.

Several PTS\_EII complexes involved in cellobiose utilization by Gram-positive bacteria were previously successfully expressed in an *E. coli* host strain (78, 79) and proven *in vitro* to be complemented by the *E. coli* EI and HPr PTS components (80). The difference in cell membrane organization between Gram positives and *E. coli* thus appears not to have an impact on the functionality of recombinant PTS\_EIIBCA complexes, even though the localization of each component of Gram-positive PTS in *E. coli* is still an open question.

**Revisiting the PTS classification.** In the last few years, a huge mass of omics data has accumulated (81), and microfluidic approaches have been developed to rapidly identify the substrates targeted by (meta)genomic loci (82). Meanwhile, an increasing number of tridimensional transporter structures have been solved (83), and the panel of biochemical methods for transporter characterization has been extended, as described in the present paper. It is thus likely that significant progress will be made over the next few years in the understanding of transporter structure-function relationships. In the present paper, we investigated this question by analyzing the diversity of

sequences and substrate specificities of known PTSs. We showed that as the number of transporters with characterized specificities increases, there is no longer a link between the names of PTS families and their functions (for example, subfamily 4.A.1.1, named “glucose subfamily” in the TCDB, contains PTSs specific to *N*-acetylglucosamine and to some glucosides, while the subfamily 4.A.1.2, named “glucoside subfamily,” contains PTSs specific to *N*-acetylmuramic acid). The present classification is thus quite confusing. Instead, we propose a transporter classification based on similarities of structures and mechanisms, with families containing members with one or more substrate specificities. This kind of classification, with no specificity-related constraints, does exist for enzymes. For example, the CAZy database, based on this principle, is a reference for carbohydrate active enzyme classification (84), even though it is complementary to the EC classification (the EC numbers now appear in the CAZy database for each biochemically characterized enzyme). For transporter classification, we recommend the continued use of the TCDB, which is a mine of information for these proteins, but with caution with respect to the level of classification. Indeed, of the five components of the transporter classification identifier (TCID), only the first two relate to structure and mechanism: the first number corresponds to the transporter class (i.e., channel, carrier [porter], primary active transporter, or group translocator), and the following letter corresponds to the transporter subclass, which in the case of primary active transporters, refers to the energy source used to drive transport. The last three TCID components are, in most cases, related to substrates (at least for PTSs) in the present TCDB. Classification into superfamilies, families, and subfamilies will thus require further global/local sequence analyses in order to identify specific common structural traits within transporter groups. Of course, listing the known substrates for each functionally characterized transporter is still highly valuable, as it will provide a clear view of the functional diversity in each of the structurally defined groups. Thus, major advances can be made to elucidate, and ultimately predict, the structural determinants of transporter specificity.

**Significance of unlocking prebiotic metabolic pathways from the human gut microbiome and implications for gut health.** FOS, one of the most commonly used and studied prebiotics, has been shown to stimulate the growth of beneficial gut bacteria such as bifidobacteria and lactic bacteria (30) but also some pathogenic *E. coli* strains (13). Previously, most of the FOS metabolization pathways were discovered from cultured bacteria, but the emergence of high-throughput functional metagenomic approaches has made it possible to study more extensive sequence spaces and highlighted new genomic loci involved in FOS metabolism by uncultured bacteria (20). Here, we studied a locus assigned to *Dorea longicatena* DSM 13814 (99% identity). However, we could not exclude that it might come from a different bacterium, which would have acquired this DNA fragment by horizontal gene transfer.

Previously, *D. longicatena* was found to be stimulated by short-chain FOS, with a poor ability to use long-chain  $\beta$ -fructans (14, 19). This is consistent with the specificity of the *Dorea* locus characterized here for kestose, a DP3 FOS, which is by far the most abundant FOS in wheat (85), a staple food for Westerners and a major component of the FOS mixtures used for dietary supplementation (86). It does not exclude the possibility, however, that other *D. longicatena* loci could be involved in FOS metabolization, since we found three other loci in strain DSM13814 harboring an I9\_GH32 homolog (33% to 42% identity) with either an ABC transporter or a PTS. *Dorea* has been shown in several studies to be positively associated with intestinal permeability in individuals with alcohol dependence, with multiple episodes of sclerosis relapse (87, 88), and with IBS (15, 16). In contrast, in several studies, it was negatively associated with IBD. This dysbiosis, which is even more pronounced in a common complication in IBD, *Clostridium difficile* infection, is likely to be due to administration of antibiotics (89, 90). At the species level, *D. longicatena* is also negatively associated with Crohn’s disease (91) and positively with remission after surgery (92). Here, however, we showed that the *Dorea* FOS utilization locus is twice as abundant in the microbiomes of patients suffering from IBD than in those of healthy individuals. It is thus difficult to correlate this

to the results of genera and species abundance in the context of IBD, especially since the present study and previous ones showed that Gram-positive and -negative PULs are frequently exchanged between gut bacteria (20, 27), providing the microbiota with metabolic flexibility and robustness. Taking that into account, it appears more informative to focus on pathology biomarkers of the microbiome and their specific functions rather than on bacterial species whose genomic composition and metabolic abilities are far from fully characterized and which are, in addition, variable.

The focus should now be on the function of the PTS characterized here and links to gut health. Based on the fact that prebiotics are characterized as stimulating the growth of beneficial gut bacteria, the effect of FOS dietary supplementation in decreasing Crohn's disease activity has been tested (93). Nevertheless, the latest results from a randomized, double-blind placebo-controlled trial revealed no significant benefit of FOS supplementation in patients with active Crohn's disease other than an induction of immunoregulatory dendritic cell responses (94). To date, only a small number of clinical trials have investigated prebiotic supplementation as treatment for chronic gastrointestinal disorders (including IBD and IBS). It remains a controversial issue with conflicting results depending on the type and dose of the prebiotic used (95). In any case, the biochemical characterization of prebiotic utilization machineries, such as the FOS-targeting transport system highlighted here both as a biomarker of diet and pathology, is of strategic importance for formulating the mechanistic bases for microbiome functional engineering, such as through the design of future specific probiotic-prebiotic combinations to maximize host benefits.

## MATERIALS AND METHODS

**Escherichia coli strains.** The metagenomic clone I9 includes contigs I9a (GenBank accession number [HE717008.1](https://www.ncbi.nlm.nih.gov/nuccore/HE717008.1)) and I9b (GenBank accession number [HE717009.1](https://www.ncbi.nlm.nih.gov/nuccore/HE717009.1)). This *E. coli* clone comes from a metagenomic library constructed by sampling the ileum mucosal microbiota of a 51-year-old male patient undergoing colonoscopy and surgery for suspected lower colon cancer (20). The metagenomic DNA fragments (30 to 40 kbp) were cloned into the pCC1FOS fosmid and transformed into the EPI100 *E. coli* strain (Epicentre Technologies). All the I9a variants were constructed using the In-Fusion HD Cloning Plus kit (Clontech) according to the instructions in the user manual. For each variant, amplification started 600 bp to 1 kb upstream of the first gene of the target locus to involve potential promoter sequences which might be necessary for gene expression (52). The primers used in this study are listed in Table S1 in the supplemental material. Mutants were confirmed by new-generation sequencing, performed by the GeT-Biopuces Platform (Toulouse) using the Ion Torrent S5 system. Read assembly was performed using Masurca (<http://www.genome.umd.edu/masurca.html>). The assembled contigs were cleaned from the pCC1FOS vector sequence using Crossmatch (<http://bozeman.mbt.washington.edu/phredphrapconsed.html>).

**Growth conditions.** All the *E. coli* variants constructed in this study were grown in M9 medium ( $\text{Na}_2\text{HPO}_4 \cdot 12\text{H}_2\text{O}$ , 17.4 g/liter;  $\text{KH}_2\text{PO}_4$ , 3.03 g/liter; NaCl, 0.51 g/liter;  $\text{NH}_4\text{Cl}$ , 2.04 g/liter;  $\text{MgSO}_4$ , 0.49 g/liter;  $\text{CaCl}_2$ , 4.38 mg/liter;  $\text{Na}_2\text{EDTA} \cdot 2\text{H}_2\text{O}$ , 15 mg/liter;  $\text{ZnSO}_4 \cdot 7\text{H}_2\text{O}$ , 4.5 mg/liter;  $\text{CoCl}_2 \cdot 6\text{H}_2\text{O}$ , 0.3 mg/liter;  $\text{MnCl}_2 \cdot 4\text{H}_2\text{O}$ , 1 mg/liter;  $\text{H}_3\text{BO}_3$ , 1 mg/liter;  $\text{Na}_2\text{MoO}_4 \cdot 2\text{H}_2\text{O}$ , 0.4 mg/liter;  $\text{FeSO}_4 \cdot 7\text{H}_2\text{O}$ , 3 mg/liter;  $\text{CuSO}_4 \cdot 5\text{H}_2\text{O}$ , 0.3 mg/liter; thiamine, 0.1 g/liter; and leucine, 0.02 g/liter) supplemented with 12.5 mg/liter chloramphenicol. The carbohydrates were diluted in M9 medium at 0.5% (wt/vol). The cultures were inoculated at an initial optical density at 600 nm ( $\text{OD}_{600}$ ) of 0.05 from precultures in LB.

Growth dynamic were analyzed at 37°C on various oligosaccharides and polysaccharides: FOS (Beghin Meiji; containing 5.3% [wt/wt] sucrose, 40.0% [wt/wt] 1-kestose, 46.0% [wt/wt] nystose, and 8.7% [wt/wt] fructosyl-nystose, quantified by HPAEC-PAD analysis, as described further in this section), sucrose (Sigma), 1-kestose (GF<sub>2</sub>; Wako Chemicals), nystose (GF<sub>3</sub>; Wako Chemicals), fructofuranosyl-nystose (GF<sub>4</sub>; Wako Chemicals), inulotriose (Megazyme), inulin from dahlia tuber (Sigma), and levan from *Erwinia herbicola* (Sigma). The optical density of the cultures was measured at 600 nm using a plate reader (Infinite M200pro; TECAN).

To evaluate the role of endogenous *E. coli* PTS genes in the phosphorylation of kestose, *E. coli* K-12 BW25113 strain and its derived single-knockout mutants (from the KEIO library) were employed (68). I9min\_PTS/GH32 fosmid was electrotransferred into *E. coli* K-12 BW25113 single-knockout mutants for the *ptsI*, *ptsH*, and *fruB* genes. Their growth abilities in M9 medium supplemented with FOS, glucose, or fructose were analyzed. The wild-type KEIO strains transformed with the I9min\_PTS/GH32 fosmid and the empty fosmid pCC1FOS were used as positive and negative controls, respectively. The cultures were inoculated at an initial optical density at  $\text{OD}_{600}$  of 0.05 from precultures in LB, and cell growth was monitored by measuring the  $\text{OD}_{600}$  over 48 h at 37°C using the FLUOStar Optima (BMG Labtech).

**FOS utilization analysis.** To determine how the different oligosaccharides in the FOS mixture were utilized by *E. coli*, HPAEC-PAD was used to measure the concentration of residual carbohydrates in the culture medium filtered at 0.20  $\mu\text{m}$ . Supernatants were analyzed on a Dionex ICS-3000 system using a CarboPac PA100 4  $\times$  250 column. Carbohydrates were eluted at 30°C at a flow rate of 1 ml/min with the

following multistep gradients: 0 to 30 min (0% to 60% B), 30 to 31 min (60% to 0% B), and 31 to 36 min (0% B). Solvents were 150 mM NaOH (eluent A) and 150 mM NaOH, 500 mM CH<sub>3</sub>COONa (eluent B).

**Enzymatic assays.** FOS hydrolysis assays were performed by using the cytoplasmic fraction of the I9min\_GH32 variant and the extracellular fraction. The I9min\_GH32 variant was grown overnight at 37°C in LB supplemented with chloramphenicol at 12.5 mg/liter. The crude cytoplasmic extracts were obtained as follows: after centrifugation, cells were concentrated to an optical density at 600 nm (OD<sub>600</sub>) of 80 in 50 mM potassium phosphate buffer (pH 7.0) containing 0.5 g/liter lysozyme and incubated at 37°C for 1 h. Cell lysis was completed with one freeze (at -80°C) and thaw (at 37°C) cycle. Cell debris was centrifuged at 15,000 × g for 30 min, and the cytoplasmic extracts were filtered with a 0.20-mm Minisart RC4 syringe filter. Enzymatic assays were performed at 37°C with either the cytoplasmic extracts or the culture supernatant and 0.5% (wt/vol) FOS, sucrose, 1-kestose, nystose, fructofuranosyl-nystose, inulotriose, inulin, or levan. Sampling was performed at the initial time point and at 24 h. Reactions were stopped by heating to 95°C for 5 min. Samples were analyzed by HPAEC-PAD as described above.

**Gene expression analysis.** Total RNAs were extracted using the RNeasy Minikit (Qiagen) from three independent cultures of the I9 clone in mid-exponential phase in LB. The RNase-free DNase set (Qiagen) was used to remove contaminating DNA. RNAs were quantified using a NanoDrop (Thermo Fisher Scientific), and the Bioanalyzer RNA kit (Agilent Technologies) was used to control their quality. Then, 5 µg of total RNA was retrotranscribed using SuperScript II reverse transcriptase (Thermo Fisher Scientific) and random primers (Invitrogen). Synthesized cDNA was purified using Illustra MicroSpin G-25 columns (GE Healthcare). The primers used for real-time quantitative PCR (qPCR) were designed using the Primer3Plus web interface with lengths from 18 to 22 bases, a GC content of more than 50%, melting temperatures between 55 and 65°C, and an amplification size from 83 to 148 bases (Table S1). Prior to RNA expression analysis, primer specificity was checked on the genomic DNA of the *E. coli* I9 clone. qPCR was carried out on a CFX96 Touch real-time PCR detection system (Bio-Rad) and monitored using the CFX Maestro software. Data were normalized based on the expression of the housekeeping gene encoding integration host factor β-subunit (*ihfB*), which is a commonly used reference gene in *E. coli* owing to its constant expression throughout growth (96). Relative expression was calculated as  $2^{-\Delta C_T}$ , in which  $\Delta C_T$  was obtained by subtracting the average cycle threshold value ( $C_{T_i}$ ; corresponding to the number of cycles required for the fluorescent signal to cross the threshold) of the housekeeping gene from that of the gene of interest (97). For each of the three biological replicates, four technical replicates were performed, corresponding to four different DNA dilutions.

**Carbohydrate uptake and binding rate quantification.** Overnight cultures of the I9min\_PTS variant in LB medium supplemented with 12.5 mg/liter chloramphenicol were centrifuged. Cells were kept at 4°C no longer than 4 h before use. For uptake experiments, cell pellets were washed three times in 50 mM Tris-buffered saline (TBS; pH 7.0) and then resuspended in TBS to reach an OD<sub>600</sub> of 40. Sucrose, fructose, glucose, kestose, nystose, fructofuranosyl-nystose, or inulotriose was added at a final concentration ranging from 0.5 to 100 mM. All reaction mixtures were incubated at 37°C with shaking at 200 rpm. After different incubation times, from 5 min to 5 h, samples of 0.2 ml were filtered with a 0.20-mm Minisart RC4 syringe filter. The concentrations of unbound carbohydrates in the supernatant were determined by HPAEC-PAD as described above. For binding experiments, cell pellets were resuspended in TBS containing 0.5 g/liter lysozyme and incubated at 37°C for 1 h. Cell lysis was completed with one freeze (at -80°C) and thaw (at 37°C) cycle. Cell membrane fractions were isolated by centrifugation at 15,000 × g for 30 min, washed three times with 50 mM Tris buffer (pH 7.0), and resuspended in the same buffer to reach an OD<sub>600</sub> of 40. The later steps were the same as for the uptake experiments. The EPI clone was used as negative control in all these experiments.

**Kestose phosphorylation analysis.** One hundred microliters of an overnight culture of a knockout *E. coli* strain in LB was used to inoculate 50-ml baffled shake flasks containing 10 ml of M9 medium supplemented with glucose or kestose as carbon sources. The flasks were incubated for 24 h at 37°C with orbital shaking at 220 rpm. Cells were harvested by centrifugation for 10 min at 2,000 × g at room temperature, washed with diluted M9, and used to inoculate 50-ml baffled shake flasks (at an OD<sub>600</sub> of 0.1) containing M9 supplemented with the same carbon source. Cell growth, performed at 37°C and 220 rpm, was monitored by measuring OD<sub>600</sub> with a cell density meter (Ultrospect 10; Amersham BioSciences). When the culture reached the exponential phase, 120 µl of culture medium was withdrawn and vigorously mixed with 1.25 ml of an acetonitrile/methanol/H<sub>2</sub>O (4:4:2) solution precooled at -20°C to rapidly quench metabolic activity and extract metabolites (67). The samples were kept at -20°C for 20 min and then centrifuged at 10,000 × g at 4°C for 10 min to remove cell debris. The supernatant was dried using a SpeedVac (SC110A SpeedVac Plus; ThermoSavant) under vacuum and then stored at -80°C until analysis.

The samples were dissolved in 120 µl of ultrapure water and then analyzed by ion chromatography (Thermo Scientific Dionex ICS-5000+ system; Dionex) coupled to an LTQ Orbitrap mass spectrometer (Thermo Fisher Scientific) equipped with an electrospray ionization probe (IC-ESI-HRMS). A revised ion chromatography method was used here (98). The KOH gradient was modified as follows: 0 min, 0.5 mM; 1 min, 0.5 mM; 9.5 min, 4.1 mM; 12.5 min, 30 mM; 24 min, 50 mM; 36 min, 60 mM; 36.1 min, 90 mM; 43 min, 90 mM; 43.5 min, 0.5 mM; 48 min, 0.5 mM. The gradients were all linear. For background suppression, an anionic electrolytically regenerated suppressor (AERS 300-2 mm; Dionex) was used. The device was operated at a constant 87-mA electrolysis current in external water mode with ultrapure water and regenerant delivered by an external AXP pump at a flow rate of 1 ml/min. The volume of the injected sample was 35 µl. Mass spectrometry analysis was performed in the negative Fourier transform mass spectrometry (FTMS) mode at a resolution of 30,000 in full scan mode with the following source



parameters: capillary temperature, 350°C; source heater temperature, 300°C; sheath gas flow rate, 50 arbitrary units (AU); auxiliary gas flow rate, 5 AU; S-Lens radio frequency (RF) level, 60%; and ion spray voltage, 3.5 kV. The data were acquired using Xcalibur software (Thermo Fisher Scientific).

**Bioinformatics analysis.** The LipoP 1.0 server was used to predict lipoprotein and signal peptides (<http://www.cbs.dtu.dk/services/LipoP/>) (99). Transmembrane domains were predicted using the TMHMM server v.2.0 (<http://www.cbs.dtu.dk/services/TMHMM/>) (100). Protein function was predicted by analyzing conserved domains in the NCBI's conserved domain database (101). Sequence similarity networks (SSNs) were generated via the Enzyme Similarity Tool (EFI-EST; <https://efi.igb.illinois.edu/efi-est/>) (102) by inputting 125 amino-acid sequences of EIIIC proteins extracted from the Transporter Classification database (TCDB; <http://www.tcdb.org/>) (103), the literature (37, 45, 104), and the present study. The SSNs were generated with edge values (E values) of  $10^{-3}$  to  $10^{-20}$ , and the alignment scores were further refined after the sequence networks were visualized in Cytoscape 3.6.1 (105). An E value threshold of  $10^{-5}$  corresponding to 21.3% sequence identity was finally used to visualize the network.

Sequences of the I9a open reading frames (ORFs) were searched by BLASTP analysis (E value = 0, identity  $\geq$  90%, no coverage threshold) against the translated catalogue of 9.9 million reference genes constructed from the fecal metagenome of 1,267 subjects from the United States, China, and Europe (46, 106). The microbial gene richness in the human gut microbiome was determined using the abundance and frequency matrix in the 1,267 subjects (<http://meta.genomics.cn/meta/dataTools>).

**Data availability.** The nucleotide sequences of the I9 metagenomic DNA are available in the GenBank database under accession numbers [HE717008.1](https://ncbi.nlm.nih.gov/nucl/HE717008.1) for contig I9a and [HE717009.1](https://ncbi.nlm.nih.gov/nucl/HE717009.1) for contig I9b.

## SUPPLEMENTAL MATERIAL

Supplemental material is available online only.

**FIG S1**, TIF file, 2.9 MB.

**FIG S2**, TIF file, 2.8 MB.

**FIG S3**, PDF file, 0.2 MB.

**FIG S4**, PDF file, 0.1 MB.

**TABLE S1**, DOCX file, 0.1 MB.

**TABLE S2**, DOCX file, 0.1 MB.

## ACKNOWLEDGMENTS

We thank Matthieu Arlat for the fruitful discussions on this project.

The analytic work was carried out with the equipment of the TBI-ICEO facility, dedicated to enzyme screening, and that of Metatoul (Metabolomics & Fluxomics Facilities, Toulouse, France; [www.metatoul.fr](http://www.metatoul.fr)). ICEO is supported by grants from the Région Midi-Pyrénées, the European Regional Development Fund, and the Institut National de la Recherche Agronomique (INRA), and MetaToul is part of the MetaboHUB-ANR-11-INBS-0010 national infrastructure ([www.metabohub.fr](http://www.metabohub.fr)).

This research was funded by the European Union's framework program Horizon 2020 (MSCA-IF-2015\_707457, CaSYS, and LEIT-BIO-2015-685474, Metafluidics). Z.W. is supported by INSA Toulouse and China Scholarship Council in the frame of the CSC-UT/INSA Program.

## REFERENCES

- Bindels LB, Delzenne NM, Cani PD, Walter J. 2015. Towards a more comprehensive concept for prebiotics. *Nat Rev Gastroenterol Hepatol* 12:303–310. <https://doi.org/10.1038/nrgastro.2015.47>.
- Wan MLY, Ling KH, El-Nezami H, Wang MF. 2019. Influence of functional food components on gut health. *Crit Rev Food Sci Nutr* 59:1927–1936. <https://doi.org/10.1080/10408398.2018.1433629>.
- Gibson GR, Hutkins R, Sanders ME, Prescott SL, Reimer RA, Salminen SJ, Scott K, Stanton C, Swanson KS, Cani PD, Verbeke K, Reid G. 2017. Expert consensus document: the International Scientific Association for Probiotics and Prebiotic (ISAPP) consensus statement on the definition and scope of prebiotics. *Nat Rev Gastroenterol Hepatol* 14:491–502. <https://doi.org/10.1038/nrgastro.2017.75>.
- Bornet FRJ, Brouns F. 2002. Immune-stimulating and gut health-promoting properties of short-chain fructo-oligosaccharides. *Nutr Rev* 60:326–334. <https://doi.org/10.1301/002966402320583442>.
- Sangeetha PT, Ramesh MN, Prapulla SG. 2005. Recent trends in the microbial production, analysis and application of fructooligosaccharides. *Trends Food Sci Technol* 16:442–457. <https://doi.org/10.1016/j.tifs.2005.05.003>.
- Akkerman R, Faas MM, de Vos P. 2019. Non-digestible carbohydrates in infant formula as substitution for human milk oligosaccharide functions: effects on microbiota and gut maturation. *Crit Rev Food Sci Nutr* 9:1486–1497. <https://doi.org/10.1080/10408398.2017.1414030>.
- Grand View Research. 2015. Inulin market by application (food & beverage, dietary supplements, pharmaceuticals) is expected to reach USD 2.35 billion by 2020. Grand View Research, Inc., San Francisco, CA.
- Grand View Research. 2016. Fructooligosaccharides (FOS) market worth \$3.52 billion By 2024. Grand View Research, Inc., San Francisco, CA.
- Gentile CL, Weir TL. 2018. The gut microbiota at the intersection of diet and human health. *Science* 362:776–780. <https://doi.org/10.1126/science.aau5812>.
- Ten Bruggencate SJM, Bovee-Oudenhoven IMJ, Lettingk-Wissink MLG, Katan MB, Van Der Meer R. 2006. Dietary fructooligosaccharides affect intestinal barrier function in healthy men. *J Nutr* 136:70–74. <https://doi.org/10.1093/jn/136.1.70>.
- Canfora EE, Jocken JW, Blaak EE. 2015. Short-chain fatty acids in control of body weight and insulin sensitivity. *Nat Rev Endocrinol* 11:577–591. <https://doi.org/10.1038/nrendo.2015.128>.
- Medina-Vera I, Sanchez-Tapia M, Noriega-López L, Granados-Portillo O, Guevara-Cruz M, Flores-López A, Avila-Nava A, Fernández ML, Tovar AR,

- Torres N. 2019. A dietary intervention with functional foods reduces metabolic endotoxaemia and attenuates biochemical abnormalities by modifying faecal microbiota in people with type 2 diabetes. *Diabetes Metab* 45:122–131. <https://doi.org/10.1016/j.diabet.2018.09.004>.
13. Mao B, Li D, Zhao J, Liu X, Gu Z, Chen YQ, Zhang H, Chen W. 2015. *In vitro* fermentation of fructooligosaccharides with human gut bacteria. *Food Funct* 6:947–954. <https://doi.org/10.1039/c4fo01082e>.
  14. Taras D, Simmering R, Collins MD, Lawson PA, Blaut M. 2002. Reclassification of *Eubacterium formicigenerans* Holdeman and Moore 1974 as *Dorea formicigenerans* gen. nov., comb. nov., and description of *Dorea longicatena* sp. nov. isolated from human. *Int J Syst Evol Microbiol* 52:423–428. <https://doi.org/10.1099/00207713-52-2-423>.
  15. Rajilić-Stojanović M, Biagi E, Heilig H, Kajander K, Kekkonen RA, Tims S, De Vos WM. 2011. Global and deep molecular analysis of microbiota signatures in fecal samples from patients with irritable bowel syndrome. *Gastroenterology* 141:1792–1801. <https://doi.org/10.1053/j.gastro.2011.07.043>.
  16. Saulnier D, Riehle K, Mistretta T, Diaz M, Mandal D, Raza S, Weidler E, Qin X, Coarfa C, Milosavljevic A, Petrosino J, Highlander S, Gibbs R, Lynch S, Shulman R, Versalovic J. 2011. Gastrointestinal microbiome signatures of pediatric patients with irritable bowel syndrome. *Gastroenterology* 141:1782–1791. <https://doi.org/10.1053/j.gastro.2011.06.072>.
  17. Harvie R, New Zealand Society of Gastroenterology, Walmsley R, Schultz M. 2017. We are what our bacteria eat: the role of bacteria in personalizing nutrition therapy in gastrointestinal conditions. *J Gastroenterol Hepatol* 32:352–357. <https://doi.org/10.1111/jgh.13462>.
  18. Chen T, Long W, Zhang C, Liu S, Zhao L, Hamaker BR. 2017. Fiber-utilizing capacity varies in *Prevotella*- versus *Bacteroides*-dominated gut microbiota. *Sci Rep* 7:2594. <https://doi.org/10.1038/s41598-017-02995-4>.
  19. Respondek F, Gerard P, Bossis M, Boschat L, Bruneau A, Rabot S, Wagner A, Martin JC. 2013. Short-chain fructo-oligosaccharides modulate intestinal microbiota and metabolic parameters of humanized gnotobiotic diet induced obesity mice. *PLoS One* 8:e71026. <https://doi.org/10.1371/journal.pone.0071026>.
  20. Cecchini DA, Laville E, Laguerre S, Robe P, Leclerc M, Doré J, Henrissat B, Remaud-Siméon M, Monsan P, Potocki-Véronèse G. 2013. Functional metagenomics reveals novel pathways of prebiotic breakdown by human gut bacteria. *PLoS One* 8:e72766. <https://doi.org/10.1371/journal.pone.0072766>.
  21. Chanteloup NK, Porcheron G, Delaleu B, Germon P, Schouler C, Moulin-Schouleur M, Gilot P. 2011. The extra-intestinal avian pathogenic *Escherichia coli* strain BEN2908 invades avian and human epithelial cells and survives intracellularly. *Vet Microbiol* 147:435–439. <https://doi.org/10.1016/j.vetmic.2010.07.013>.
  22. Schouler C, Taki A, Chouikha I, Moulin-Schouleur M, Gilot P. 2008. A genomic island of an extraintestinal pathogenic *Escherichia coli* strain enables the metabolism of fructooligosaccharides, which improves intestinal colonization. *J Bacteriol* 191:388–393. <https://doi.org/10.1128/JB.01052-08>.
  23. Lombard V, Golaconda Ramulu H, Drula E, Coutinho PM, Henrissat B. 2014. The carbohydrate-active enzymes database (CAZy) in 2013. *Nucleic Acids Res* 42:D490–D495. <https://doi.org/10.1093/nar/gkt1178>.
  24. Flint HJ, Bayer EA, Rincon MT, Lamed R, White BA. 2008. Polysaccharide utilization by gut bacteria: potential for new insights from genomic analysis. *Nat Rev Microbiol* 6:121–131. <https://doi.org/10.1038/nrmicro1817>.
  25. Koropatkin NM, Cameron EA, Martens EC. 2012. How glycan metabolism shapes the human gut microbiota. *Nat Rev Microbiol* 10:323–335. <https://doi.org/10.1038/nrmicro2746>.
  26. Foley MH, Cockburn DW, Koropatkin NM. 2016. The Sus operon: a model system for starch uptake by the human gut Bacteroidetes. *Cell Mol Life Sci* 73:2603–2617. <https://doi.org/10.1007/s00018-016-2242-x>.
  27. Tasse L, Bercovic J, Pizzut-Serin S, Robe P, Tap J, Klopp C, Cantarel BL, Coutinho PM, Henrissat B, Leclerc M, Doré J, Monsan P, Remaud-Simeon M, Potocki-Veronese G. 2010. Functional metagenomics to mine the human gut microbiome for dietary fiber catabolic enzymes. *Genome Res* 20:1605–1612. <https://doi.org/10.1101/gr.108332.110>.
  28. Terrapon N, Lombard V, Drula E, Lapébie P, Al-Masaudi S, Gilbert HJ, Henrissat B. 2018. PULDB: the expanded database of polysaccharide utilization loci. *Nucleic Acids Res* 46:D677–D683. <https://doi.org/10.1093/nar/gkx1022>.
  29. Sheridan PO, Martin JC, Lawley TD, Browne HP, Harris HMB, Bernalier-Donadille A, Duncan SH, O'Toole PW, Scott KP, Flint HJ. 2016. Polysaccharide utilization loci and nutritional specialization in a dominant group of butyrate-producing human colonic *Firmicutes*. *Microb Genom* 2:e000043. <https://doi.org/10.1099/mgen.0.000043>.
  30. Goh YJ, Klaenhammer TR. 2015. Genetic mechanisms of prebiotic oligosaccharide metabolism in probiotic microbes. *Annu Rev Food Sci Technol* 6:137–156. <https://doi.org/10.1146/annurev-food-022814-015706>.
  31. Sonnenburg ED, Zheng H, Joglekar P, Higginbottom SK, Firkbank SJ, Bolam DN, Sonnenburg JL. 2010. Specificity of polysaccharide use in intestinal bacteroides species determines diet-induced microbiota alterations. *Cell* 141:1241–1252. <https://doi.org/10.1016/j.cell.2010.05.005>.
  32. Joglekar P, Sonnenburg ED, Higginbottom SK, Earle KA, Morland C, Shapiro-Ward S, Bolam DN, Sonnenburg JL, Abbott W, Koropatkin N. 2018. Genetic variation of the SusC/SusD homologs from a polysaccharide utilization locus underlies divergent fructan specificities and functional adaptation in *Bacteroides thetaiotaomicron* strains. *mSphere* 3:e00185-18. <https://doi.org/10.1128/mSphereDirect.00185-18>.
  33. Boger MCL, Lammerts van Bueren A, Dijkhuizen L. 2018. Cross-feeding amongst probiotic bacterial strains on prebiotic inulin involving the extracellular exo-inulinase of *Lactobacillus paracasei* strain W20. *Appl Environ Microbiol* 84:e01539-18. <https://doi.org/10.1128/AEM.01539-18>.
  34. Vijayaraghavan K, Yamini D, Ambika V, Sravya Sowdamini N. 2009. Trends in inulinase production—a review. *Crit Rev Biotechnol* 29:67–77. <https://doi.org/10.1080/0738850802685389>.
  35. Barrangou R, Altermann E, Hutkins R, Cano R, Klaenhammer TR. 2003. Functional and comparative genomic analyses of an operon involved in fructooligosaccharide utilization by *Lactobacillus acidophilus*. *Proc Natl Acad Sci U S A* 100:8957–8962. <https://doi.org/10.1073/pnas.1332765100>.
  36. Linke CM, Woodiga SA, Meyers DJ, Buckwalter CM, Salhi HE, King SJ. 2013. The ABC transporter encoded at the pneumococcal fructooligosaccharide utilization locus determines the ability to utilize long- and short-chain fructooligosaccharides. *J Bacteriol* 195:1031–1041. <https://doi.org/10.1128/JB.01560-12>.
  37. Chen C, Zhao G, Chen W, Guo B. 2015. Metabolism of fructooligosaccharides in *Lactobacillus plantarum* ST-III via differential gene transcription and alteration of cell membrane fluidity. *Appl Environ Microbiol* 81:7697–7707. <https://doi.org/10.1128/AEM.02426-15>.
  38. Cockburn DW, Koropatkin NM. 2016. Polysaccharide degradation by the intestinal microbiota and its influence on human health and disease. *J Mol Biol* 428:3230–3252. <https://doi.org/10.1016/j.jmb.2016.06.021>.
  39. Grondin JM, Tamura K, Déjean G, Abbott DW, Brumer H. 2017. Polysaccharide utilization loci: fueling microbial communities. *J Bacteriol* 199:e00860-16. <https://doi.org/10.1128/JB.00860-16>.
  40. van de Guchte M, Blottière HM, Doré J. 2018. Humans as holobionts: implications for prevention and therapy. *Microbiome* 6:81. <https://doi.org/10.1186/s40168-018-0466-8>.
  41. Deutscher J, Aké FMD, Derkaoui M, Zébré AC, Cao TN, Bouraoui H, Kentache T, Mokhtari A, Milohanic E, Joyet P. 2014. The bacterial phosphoenolpyruvate:carbohydrate phosphotransferase system: regulation by protein phosphorylation and phosphorylation-dependent protein-protein interactions. *Microbiol Mol Biol Rev* 78:231–256. <https://doi.org/10.1128/MMBR.00001-14>.
  42. Keyhani NO, Wang LX, Lee YC, Roseman S. 2000. The chitin disaccharide, *N,N'*-diacetylchitobiose, is catabolized by *Escherichia coli* and is transported/phosphorylated by the phosphoenolpyruvate:glycose phosphotransferase system. *J Biol Chem* 275:33084–33090. <https://doi.org/10.1074/jbc.M001043200>.
  43. Tchiew JH, Norris V, Edwards JS, Saier MH. 2001. The complete phosphotransferase system in *Escherichia coli*. *J Mol Microbiol Biotechnol* 3:329–346.
  44. Mo S, Kim BS, Yun SJ, Lee JJ, Yoon SH, Oh CH. 2015. Genome sequencing of *Clostridium butyricum* DKU-01, isolated from infant feces. *Gut Pathog* 7:8. <https://doi.org/10.1186/s13099-015-0055-3>.
  45. Saulnier DMA, Molenaar D, De Vos WM, Gibson GR, Kolida S. 2007. Identification of prebiotic fructooligosaccharide metabolism in *Lactobacillus plantarum* WCFS1 through microarrays. *Appl Environ Microbiol* 73:1753–1765. <https://doi.org/10.1128/AEM.01151-06>.
  46. Li J, Jia H, Cai X, Zhong H, Feng Q, Sunagawa S, Arumugam M, Kultima

- JR, Prifti E, Nielsen T, Juncker AS, Manichanh C, Chen B, Zhang W, Levenez F, Wang J, Xu X, Xiao L, Liang S, Zhang D, Zhang Z, Chen W, Zhao H, Al-Aama JY, Edris S, Yang H, Wang J, Hansen T, Nielsen HB, Brunak S, Kristiansen K, Guarner F, Pedersen O, Doré J, Ehrlich SD, Bork P, Wang J, MetaHIT Consortium. 2014. An integrated catalog of reference genes in the human gut microbiome. *Nat Biotechnol* 32:834–841. <https://doi.org/10.1038/nbt.2942>.
47. Sun D. 2018. Pull in and push out: mechanisms of horizontal gene transfer in bacteria. *Front Microbiol* 9:2154. <https://doi.org/10.3389/fmicb.2018.02154>.
  48. O'Connor Á. 2012. Bread consumption in the UK: what are the main attitudinal factors affecting current intake and its place in a healthy diet? *Nutr Bull* 37:368–379. <https://doi.org/10.1111/j.1467-3010.2012.01989.x>.
  49. Notarnicola B, Tassielli G, Renzulli PA, Monforti F. 2017. Energy flows and greenhouses gases of EU (European Union) national breads using an LCA (life cycle assessment) approach. *J Clean Prod* 140:455–469. <https://doi.org/10.1016/j.jclepro.2016.05.150>.
  50. Lipoeto NI, Geok Lin K, Angeles-Agdeppa I. 2013. Food consumption patterns and nutrition transition in South-East Asia. *Public Health Nutr* 16:1637–1643. <https://doi.org/10.1017/S1368980012004569>.
  51. Hu EA, Pan A, Malik V, Sun Q. 2012. White rice consumption and risk of type 2 diabetes: meta-analysis and systematic review. *BMJ* 344:e1454. <https://doi.org/10.1136/bmj.e1454>.
  52. Tauzin AS, Laville E, Xiao Y, Nouaille S, Le Bourgeois P, Heux S, Portais JC, Monsan P, Martens EC, Potocki-Veronese G, Bordes F. 2016. Functional characterization of a gene locus from an uncultured gut *Bacteroides* conferring xylo-oligosaccharides utilization to *Escherichia coli*. *Mol Microbiol* 102:579–592. <https://doi.org/10.1111/mmi.13480>.
  53. Locher KP. 2016. Mechanistic diversity in ATP-binding cassette (ABC) transporters. *Nat Struct Mol Biol* 23:487–493. <https://doi.org/10.1038/nsmb.3216>.
  54. Rice AJ, Park A, Pinkett HW. 2014. Diversity in ABC transporters: type I, II and III importers. *Crit Rev Biochem Mol Biol* 49:426–437. <https://doi.org/10.3109/10409238.2014.953626>.
  55. Solopova A, Bachmann H, Teusink B, Kok J, Kuipers OP. 2018. Further elucidation of galactose utilization in *Lactococcus lactis* MG1363. *Front Microbiol* 9:1803. <https://doi.org/10.3389/fmicb.2018.01803>.
  56. Cao Y, Jin X, Levin EJ, Huang H, Zong Y, Quick M, Weng J, Pan Y, Love J, Punta M, Rost B, Hendrickson WA, Javitch JA, Rajashankar KR, Zhou M. 2011. Crystal structure of a phosphorylation-coupled saccharide transporter. *Nature* 473:50–54. <https://doi.org/10.1038/nature09939>.
  57. Martens EC, Chiang HC, Gordon JI. 2008. Mucosal glycan foraging enhances fitness and transmission of a saccharolytic human gut bacterial symbiont. *Cell Host Microbe* 4:447–457. <https://doi.org/10.1016/j.chom.2008.09.007>.
  58. Schwalm ND, Groisman EA. 2017. Navigating the gut buffet: control of polysaccharide utilization in *Bacteroides* spp. *Trends Microbiol* 25:1005–1015. <https://doi.org/10.1016/j.tim.2017.06.009>.
  59. Tauzin AS, Kwiatkowski KJ, Orlovsky NI, Smith CJ, Creagh AL, Haynes CA, Wawrzak Z, Brumer H, Koropatkin NM. 2016. Molecular dissection of xyloglucan recognition in a prominent human gut symbiont. *mBio* 7:e02134-15. <https://doi.org/10.1128/mBio.02134-15>.
  60. Culurgioni S, Harris G, Singh AK, King SJ, Walsh MA. 2017. Structural basis for regulation and specificity of fructooligosaccharide import in *Streptococcus pneumoniae*. *Structure* 25:79–93. <https://doi.org/10.1016/j.str.2016.11.008>.
  61. Jeckelmann JM, Harder D, Mari SA, Meury M, Ucurum Z, Müller DJ, Erni B, Fotiadis D. 2011. Structure and function of the glucose PTS transporter from *Escherichia coli*. *J Struct Biol* 176:395–403. <https://doi.org/10.1016/j.jsb.2011.09.012>.
  62. Keyhani NO, Wang L-X, Lee YC, Roseman S. 1996. The chitin catabolic cascade in the marine bacterium *Vibrio furnissii*. *J Biol Chem* 271:33409–33413. <https://doi.org/10.1074/jbc.271.52.33409>.
  63. Chen L-Q, Cheung LS, Feng L, Tanner W, Frommer WB. 2015. Transport of sugars. *Annu Rev Biochem* 84:865–894. <https://doi.org/10.1146/annurev-biochem-060614-033904>.
  64. Miller DM, Olson JS, Pflugrath JW, Quijcho FA. 1983. Rates of ligand binding to periplasmic proteins involved in bacterial transport and chemotaxis. *J Biol Chem* 258:13665–13672.
  65. Lendenmann U, Snozzi M, Egli T. 1999. Growth kinetics of *Escherichia coli* with galactose and several other sugars in carbon-limited chemostat culture. *Can J Microbiol* 46:72–80. <https://doi.org/10.1139/w99-113>.
  66. Senn H, Lendenmann U, Snozzi M, Hamer G, Egli T. 1994. The growth of *Escherichia coli* in glucose-limited chemostat cultures: a re-examination of the kinetics. *Biochim Biophys Acta* 1201:424–436. [https://doi.org/10.1016/0304-4165\(94\)90072-8](https://doi.org/10.1016/0304-4165(94)90072-8).
  67. Millard P, Massou S, Wittmann C, Portais JC, Létisse F. 2014. Sampling of intracellular metabolites for stationary and non-stationary <sup>13</sup>C metabolic flux analysis in *Escherichia coli*. *Anal Biochem* 465:38–49. <https://doi.org/10.1016/j.ab.2014.07.026>.
  68. Baba T, Ara T, Hasegawa M, Takai Y, Okumura Y, Baba M, Datsenko KA, Tomita M, Wanner BL, Mori H. 2006. Construction of *Escherichia coli* K-12 in-frame, single-gene knockout mutants: the Keio collection. *Mol Syst Biol* 2:2006:0008. <https://doi.org/10.1038/msb4100050>.
  69. Saier MH, Tran CV, Barabote RD. 2006. TCDB: the Transporter Classification Database for membrane transport protein analyses and information. *Nucleic Acids Res* 34:D181–D186. <https://doi.org/10.1093/nar/gkj001>.
  70. Nguyen TX, Yen MR, Barabote RD, Saier MH. 2006. Topological predictions for integral membrane permeases of the phosphoenolpyruvate: sugar phosphotransferase system. *J Mol Microbiol Biotechnol* 11:345–360. <https://doi.org/10.1159/000095636>.
  71. Tarpan MA, De Cooman H, Sagstuen E, Waroquier M, Callens F. 2011. Identification of primary free radicals in trehalose dihydrate single crystals X-irradiated at 10 K. *Phys Chem Chem Phys* 13:11294–11302. <https://doi.org/10.1039/c0cp02616f>.
  72. El-Gebali S, Mistry J, Bateman A, Eddy SR, Luciani A, Potter SC, Qureshi M, Richardson LJ, Salazar GA, Smart A, Sonnhammer ELL, Hirsh L, Paladin L, Piovesan D, Tosatto SCE, Finn RD. 2019. The Pfam protein families database in 2019. *Nucleic Acids Res* 47:D427–D432. <https://doi.org/10.1093/nar/gky995>.
  73. Mukherjee S, Stamatis D, Bertsch J, Ovchinnikova G, Katta HY, Mojica A, Chen IMA, Kyripides NC, Reddy T. 2019. Genomes Online database (GOLD) v.7: updates and new features. *Nucleic Acids Res* 47:D649–D659. <https://doi.org/10.1093/nar/gky977>.
  74. Lapébie P, Lombard V, Drula E, Terrapon N, Henrissat B. 2019. Bacteroidetes use thousands of enzyme combinations to break down glycans. *Nat Commun* 10:2043. <https://doi.org/10.1038/s41467-019-10068-5>.
  75. O' Donnell MM, Forde BM, Neville B, Ross PR, O' Toole PW. 2011. Carbohydrate catabolic flexibility in the mammalian intestinal commensal *Lactobacillus ruminis* revealed by fermentation studies aligned to genome annotations. *Microb Cell Fact* 10 Suppl 1:S12. <https://doi.org/10.1186/1475-2859-10-S1-S12>.
  76. Barrangou R, Azcarate-Peril MA, Duong T, Conners SB, Kelly RM, Klaenhammer TR. 2006. Global analysis of carbohydrate utilization by *Lactobacillus acidophilus* using cDNA microarrays. *Proc Natl Acad Sci U S A* 103:3816–3821. <https://doi.org/10.1073/pnas.0511287103>.
  77. Veldhuis G, Broos J, Poolman B, Scheek RM. 2005. Stoichiometry and substrate affinity of the mannitol transporter, enzymell<sup>TM</sup>, from *Escherichia coli*. *Biophys J* 89:201–210. <https://doi.org/10.1529/biophysj.105.062877>.
  78. Lai X, Ingram LO. 1993. Cloning and sequencing of a cellobiose phosphotransferase system operon from *Bacillus stearothermophilus* XL-65-6 and functional expression in *Escherichia coli*. *J Bacteriol* 175:6441–6450. <https://doi.org/10.1128/jb.175.20.6441-6450.1993>.
  79. Lai X, Davis FV, Hespell RB, Ingram LO. 1997. Cloning of cellobiose phosphoenolpyruvate-dependent phosphotransferase genes: functional expression in recombinant. *Appl Environ Microbiol* 63:355–363.
  80. Zheng Z, Jiang T, Zou L, Ouyang S, Zhou J, Lin X, He Q, Wang L, Yu B, Xu H, Ouyang J. 2018. Simultaneous consumption of cellobiose and xylose by *Bacillus coagulans* to circumvent glucose repression and identification of its cellobiose-assimilating operons. *Biotechnol Biofuels* 11:320. <https://doi.org/10.1186/s13068-018-1323-5>.
  81. Kappelmann L, Krüger K, Hehemann JH, Harder J, Markert S, Unfried F, Becher D, Shapiro N, Schweder T, Amann RI, Teeling H. 2019. Polysaccharide utilization loci of North Sea *Flavobacteriia* as basis for using SusC/D-protein expression for predicting major phytoplankton glycans. *ISME J* 13:76–91. <https://doi.org/10.1038/s41396-018-0242-6>.
  82. Dagkesamanskaya A, Langer K, Tauzin AS, Rouzeau C, Lestrade D, Potocki-Veronese G, Boitard L, Bibette J, Baudry J, Pompon D, Anton-Lebere V. 2018. Use of photoswitchable fluorescent proteins for droplet-based microfluidic screening. *J Microbiol Methods* 147:59–65. <https://doi.org/10.1016/j.mimet.2018.03.001>.
  83. Glenwright AJ, Pothula KR, Bhamidimarri SP, Chorev DS, Baslé A, Firbank SJ, Zheng H, Robinson CV, Winterhalter M, Kleinekathöfer U,



- Bolam DN, van den Berg B. 2017. Structural basis for nutrient acquisition by dominant members of the human gut microbiota. *Nature* 541:407–411. <https://doi.org/10.1038/nature20828>.
84. Henrissat B. 1991. A classification of glycosyl hydrolases based on amino acid sequence similarities. *Biochem J* 280:309–316. <https://doi.org/10.1042/bj2800309>.
  85. Hussein HS, Campbell JM, Bauer LL, Fahey GC, Hogarth A, Wolf BW, Hunter DE. 1998. Selected fructooligosaccharide composition of pet-food ingredients. *J Nutr* 128:2803S–2805S. <https://doi.org/10.1093/jn/128.12.2803S>.
  86. Korakli M, Hinrichs C, Ehrmann MA, Vogel RF. 2003. Enzymatic determination of inulin and fructooligosaccharides in food. *Eur Food Res Technol* 217:530–534. <https://doi.org/10.1007/s00217-003-0803-3>.
  87. Chen J, Chia N, Kalari KR, Yao JZ, Novotna M, Soldan MMP, Luckey DH, Marietta EV, Jeraldo PR, Chen X, Weinschenker BG, Rodriguez M, Kantarci OH, Nelson H, Murray JA, Mangalam AK. 2016. Multiple sclerosis patients have a distinct gut microbiota compared to healthy controls. *Sci Rep* 6:28484–28410. <https://doi.org/10.1038/srep28484>.
  88. Leclercq S, Matamoros S, Cani PD, Neyrinck AM, Jamar F, Stärkel P, Windey K, Tremaroli V, Bäckhed F, Verbeke K, de Timary P, Delzenne NM. 2014. Intestinal permeability, gut-bacterial dysbiosis, and behavioral markers of alcohol-dependence severity. *Proc Natl Acad Sci U S A* 111:E4485–E4493. <https://doi.org/10.1073/pnas.1415174111>.
  89. Sokol H, Leducq V, Aschard H, Pham HP, Jegou S, Landman C, Cohen D, Liguori G, Bourrier A, Nion-Larmurier I, Cosnes J, Seksik P, Langella P, Skurnik D, Richard ML, Beaugerie L. 2017. Fungal microbiota dysbiosis in IBD. *Gut* 66:1039–1048. <https://doi.org/10.1136/gutjnl-2015-310746>.
  90. Morgan XC, Tickle TL, Sokol H, Gevers D, Devaney KL, Ward DV, Reyes JA, Shah SA, LeLeiko N, Snapper SB, Bousvaros A, Korzenik J, Sands BE, Xavier RJ, Huttenhower C. 2012. Dysfunction of the intestinal microbiome in inflammatory bowel disease and treatment. *Genome Biol* 13:R79. <https://doi.org/10.1186/gb-2012-13-9-r79>.
  91. Gupta A, Kang S, Wagner J, Kirkwood CD, Morrison M, McSweeney C, Finlay M. 2014. Analysis of mucosal microbiota in inflammatory bowel disease using a custom phylogenetic microarray. *Austin J Gastroenterol* 1:1020.
  92. Mondot S, Lepage P, Seksik P, Allez M, Tréton X, Bouhnik Y, Colombel JF, Leclerc M, Pochart P, Doré J, Marteau P, GETAID. 2016. Structural robustness of the gut mucosal microbiota is associated with Crohn's disease remission after surgery. *Gut* 65:954–962. <https://doi.org/10.1136/gutjnl-2015-309184>.
  93. Lindsay JO, Whelan K, Stagg AJ, Gobin P, Al-Hassi HO, Rayment N, Kamm MA, Knight SC, Forbes A. 2006. Clinical, microbiological, and immunological effects of fructo-oligosaccharide in patients with Crohn's disease. *Gut* 55:348–355. <https://doi.org/10.1136/gut.2005.074971>.
  94. Benjamin JL, Hedin CRH, Koutsoumpas A, Ng SC, McCarthy NE, Hart AL, Kamm MA, Sanderson JD, Knight SC, Forbes A, Stagg AJ, Whelan K, Lindsay JO. 2011. Randomised, double-blind, placebo-controlled trial of fructo-oligosaccharides in active Crohn's disease. *Gut* 60:923–929. <https://doi.org/10.1136/gut.2010.232025>.
  95. Wilson B, Whelan K. 2017. Prebiotic inulin-type fructans and galactooligosaccharides: definition, specificity, function, and application in gastrointestinal disorders. *J Gastroenterol Hepatol* 32:64–68. <https://doi.org/10.1111/jgh.13700>.
  96. Wegleńska A, Jacob B, Sirko A. 1996. Transcriptional pattern of *Escherichia coli ihfB (himD)* gene expression. *Gene* 181:85–88. [https://doi.org/10.1016/s0378-1119\(96\)00468-4](https://doi.org/10.1016/s0378-1119(96)00468-4).
  97. Livak KJ, Schmittgen TD. 2001. Analysis of relative gene expression data using real-time quantitative PCR and the  $2^{-\Delta\Delta CT}$  method. *Methods* 25:402–408. <https://doi.org/10.1006/meth.2001.1262>.
  98. Kiefer P, Nicolas C, Létisse F, Portais JC. 2007. Determination of carbon labeling distribution of intracellular metabolites from single fragment ions by ion chromatography tandem mass spectrometry. *Anal Biochem* 360:182–188. <https://doi.org/10.1016/j.ab.2006.06.032>.
  99. Rahman O, Cummings SP, Harrington DJ, Sutcliffe IC. 2008. Methods for the bioinformatic identification of bacterial lipoproteins encoded in the genomes of Gram-positive bacteria. *World J Microbiol Biotechnol* 24:2377–2382. <https://doi.org/10.1007/s11274-008-9795-2>.
  100. Krogh A, Larsson B, Von Heijne G, Sonnhammer E. 2001. Predicting transmembrane protein topology with a hidden Markov model: application to complete genomes. *J Mol Biol* 305:567–580. <https://doi.org/10.1006/jmbi.2000.4315>.
  101. Marchler-Bauer A, Bo Y, Han L, He J, Lanczycki CJ, Lu S, Chitsaz F, Derbyshire MK, Geer RC, Gonzales NR, Gwadz M, Hurwitz DI, Lu F, Marchler GH, Song JS, Thanki N, Wang Z, Yamashita RA, Zhang D, Zheng C, Geer LY, Bryant SH. 2017. CDD/SPARCLE: functional classification of proteins via subfamily domain architectures. *Nucleic Acids Res* 45:D200–D203. <https://doi.org/10.1093/nar/gkw1129>.
  102. Gerlt JA, Bouvier JT, Davidson DB, Imker HJ, Sadkhin B, Slater DR, Whalen KL. 2015. Enzyme function initiative-enzyme similarity tool (EFI-EST): a web tool for generating protein sequence similarity networks. *Biochim Biophys Acta* 1854:1019–1037. <https://doi.org/10.1016/j.bbapap.2015.04.015>.
  103. Saier MH, Reddy VS, Tsu BV, Ahmed MS, Li C, Moreno-Hagelsieb G. 2016. The Transporter Classification Database (TCDB): recent advances. *Nucleic Acids Res* 44:D372–D379. <https://doi.org/10.1093/nar/gkv1103>.
  104. Iyer R, Camilli A. 2007. Sucrose metabolism contributes to *in vivo* fitness of *Streptococcus pneumoniae*. *Mol Microbiol* 66:1–13. <https://doi.org/10.1111/j.1365-2958.2007.05878.x>.
  105. Shannon P, Markiel A, Ozier O, Baliga NS, Wang JT, Ramage D, Amin N, Schwikowski B, Ideker T. 2003. Cytoscape: a software environment for integrated models of biomolecular interaction networks. *Genome Res* 13:2498–2504. <https://doi.org/10.1101/gr.1239303>.
  106. Altschul SF, Gish W, Miller W, Myers EW, Lipman DJ. 1990. Basic local alignment search tool. *J Mol Biol* 215:403–410. [https://doi.org/10.1016/S0022-2836\(05\)80360-2](https://doi.org/10.1016/S0022-2836(05)80360-2).